

University of Windsor

Scholarship at UWindsor

Electronic Theses and Dissertations

Theses, Dissertations, and Major Papers

2005

Development of an advanced aluminum thermal analysis system for the characterization of the 319 aluminum alloy solidification process.

Todd J. Stockwell
University of Windsor

Follow this and additional works at: <https://scholar.uwindsor.ca/etd>

Recommended Citation

Stockwell, Todd J., "Development of an advanced aluminum thermal analysis system for the characterization of the 319 aluminum alloy solidification process." (2005). *Electronic Theses and Dissertations*. 1711.

<https://scholar.uwindsor.ca/etd/1711>

This online database contains the full-text of PhD dissertations and Masters' theses of University of Windsor students from 1954 forward. These documents are made available for personal study and research purposes only, in accordance with the Canadian Copyright Act and the Creative Commons license—CC BY-NC-ND (Attribution, Non-Commercial, No Derivative Works). Under this license, works must always be attributed to the copyright holder (original author), cannot be used for any commercial purposes, and may not be altered. Any other use would require the permission of the copyright holder. Students may inquire about withdrawing their dissertation and/or thesis from this database. For additional inquiries, please contact the repository administrator via email (scholarship@uwindsor.ca) or by telephone at 519-253-3000ext. 3208.

NOTE TO USERS

This reproduction is the best copy available.

UMI[®]

**Development of an Advanced Aluminum Thermal Analysis System for the
Characterization of the 319 Aluminum Alloy Solidification Process**

By

Todd J. Stockwell

A Thesis

Submitted to the College of Graduate Studies and Research
Through the Engineering Materials Graduate Program in the
College of Engineering in Partial Fulfillment of the Requirements
for the Degree of Master of Applied Science in Engineering Materials
at the University of Windsor

Windsor, Ontario, Canada 1999

© T.J. STOCKWELL 1999



Library and
Archives Canada

Bibliothèque et
Archives Canada

Published Heritage
Branch

Direction du
Patrimoine de l'édition

395 Wellington Street
Ottawa ON K1A 0N4
Canada

395, rue Wellington
Ottawa ON K1A 0N4
Canada

Your file *Votre référence*

ISBN: 0-494-09800-7

Our file *Notre référence*

ISBN: 0-494-09800-7

NOTICE:

The author has granted a non-exclusive license allowing Library and Archives Canada to reproduce, publish, archive, preserve, conserve, communicate to the public by telecommunication or on the Internet, loan, distribute and sell theses worldwide, for commercial or non-commercial purposes, in microform, paper, electronic and/or any other formats.

The author retains copyright ownership and moral rights in this thesis. Neither the thesis nor substantial extracts from it may be printed or otherwise reproduced without the author's permission.

AVIS:

L'auteur a accordé une licence non exclusive permettant à la Bibliothèque et Archives Canada de reproduire, publier, archiver, sauvegarder, conserver, transmettre au public par télécommunication ou par l'Internet, prêter, distribuer et vendre des thèses partout dans le monde, à des fins commerciales ou autres, sur support microforme, papier, électronique et/ou autres formats.

L'auteur conserve la propriété du droit d'auteur et des droits moraux qui protègent cette thèse. Ni la thèse ni des extraits substantiels de celle-ci ne doivent être imprimés ou autrement reproduits sans son autorisation.

In compliance with the Canadian Privacy Act some supporting forms may have been removed from this thesis.

Conformément à la loi canadienne sur la protection de la vie privée, quelques formulaires secondaires ont été enlevés de cette thèse.

While these forms may be included in the document page count, their removal does not represent any loss of content from the thesis.

Bien que ces formulaires aient inclus dans la pagination, il n'y aura aucun contenu manquant.


Canada

Abstract

Thermal analysis is the study of heat evolution as a molten alloy transforms to a solid. Studying the evolution of heat results in a temperature, time relationship in the form of a cooling curve. Specific characteristics of the 319-aluminum cooling curve are described and related to specific metallurgical properties. Variations in the cooling curves represent changes within the solidification of the alloy and are correlated to changes in the metallurgical properties.

In the present work, an aluminum thermal analysis system (ALTAS) is constructed to withstand the rigors of day to day foundry conditions. Complete automation has been introduced to reduce the number of variables introduced by the operator to the system. This includes automatic analysis and storage of the results in a database, which allows for later statistical evaluation. Methods of noise filtering and automatic temperature detection have all been improved over previous systems in order to reduce measurement error.

Experimental work concluded that ALTAS is capable of determining the degree of silicon modification as a result of strontium additions. In addition, ALTAS is able to determine which aluminum-copper phases are present including the area fraction of each in the aluminum 319 alloy.

Acknowledgments

I would like to thank my advisor Dr. J.H. Sokolowski, Drs. W. Kierkus, M. Djurdjevic and the rest of the IRC team for their advice, guidance and friendship throughout this investigation. I would also like to thank Jim Hochreiter and the Technical Support Centre for their hard work in the programming and construction of AITAS. The contributions they have made are innumerable and greatly appreciated. Finally, I would like to thank the Ford Motor Company and the Natural Sciences and Engineering Research Council of Canada for their support of this work.

Table of Contents

Abstract	ii
Acknowledgements	iii
Table of Contents	iv
List of Figures	viii
List of Tables	xi
Chapter 1. Introduction	1
1.1. Background	1
1.2. Objectives of this Work	2
Chapter 2. Literature Review	3
2.1. Thermal Analysis of Binary Alloys	3
2.2. Binary Aluminum – Silicon Phase Diagram	4
2.3. Aluminum – Silicon Foundry Alloys	5
2.4. Review of Thermodynamics	6
2.5. Nucleation	8
Chapter 3. AITAS – Aluminum Thermal Analysis System	11
3.1. AITAS Hardware	11
3.2. AITAS Software Capabilities	13

3.3.	AITAS System for The Ford Windsor Aluminum Plant and Casting Process and Development Centre	14
3.4.	System for “On The Floor” Use	15
3.5.	Advanced Engineering System	16
3.6.	AITAS for the Continuous Advancement of Thermal Analysis	16
3.7.	Signal Processing	17
3.7.1.	Introduction	17
3.7.2.	Moving Average Filtering	17
3.7.3.	Weighted Moving Average Filtering	21
3.7.4.	Incorporation of Weighted Moving Average Filtering into AITAS	25
Chapter 4.	Analysis of Cooling Curve	26
4.1.	Background	26
4.2.	Region I – Liquidus and Dendrite Coherency	28
4.3.	Region II – Al-Si Eutectic	31
4.4.	Region III – Low Melting Temperature Al ₂ Cu and Al-Cu-Si-Mg Eutectic Reactions and the End of the Solidification Process	33
4.5.	Assessment of Grain Size	35
4.5.1.	Literature Search	35
4.5.2.	AITAS Determination of Grain Size Refinement	40

Chapter 5.	The Effect of Strontium Additions on Aluminum – Silicon Modification	41
5.1.	Silicon Modification Literature Search	41
5.2.	AITAS Determination of Silicon Modification	43
5.3.	Experimental Work	43
5.3.1.	Objectives	43
5.3.2.	Experimental Procedure	44
5.3.3.	Results	45
5.3.4.	Conclusions	48
Chapter 6.	The Effect of Strontium on the Formation of Al-Cu Phases	49
6.1.	Literature Search	49
6.2.	Experimental Work	50
6.2.1.	Objective	50
6.2.2.	Experimental Procedure	50
6.2.3.	Results	51
6.2.4.	Conclusions	53
Chapter 7.	Modeling of Fraction Solid	54
7.1.	Literature Search	54
7.2.	Experimental Work	56
7.2.1.	Objectives	56
7.2.2.	Experimental Procedure	56

7.2.3.	Results	57
7.2.4.	Conclusions	62
Chapter 8.	Conclusions and Recommendations	63
References		64
Appendix A –	AITAS Training Manual	67
Vita Auctoris		94

List of Figures

Figure 2.1 - Cooling curve of an Al-Si binary alloy	3
Figure 2.2 - Diagram showing how cooling curve analysis information is transferred to a phase diagram	4
Figure 2.3 - Al-Si phase diagram	5
Figure 2.4 - Pressure-temperature phase diagram for a single component system including isobars [38]	7
Figure 2.5 - Free energy curves for the phases in a one component system at three different pressures [38]	7
Figure 2.6 - Free energy of a particle as a function of radius [38]	8
Figure 3.1 - ALTAS stand	12
Figure 3.2 - Schematic of thermal analysis test sample	12
Figure 3.3 - Schematic of data flow	15
Figure 3.4 - Original cooling curve showing region of analysis.	20
Figure 3.5 - Original curve and moving average with a window length of 11 (Bessel shown for comparison)	20
Figure 3.6 - Original curve and moving average with a window length of 31 (Bessel shown for comparison)	21
Figure 3.7 - Cooling curve with moving average and weighted moving average filtered versions, with a window length of 51	23
Figure 3.8 - Cooling curve with moving average and weighted moving average filtered versions, with a window length of 81	23
Figure 3.9 - Cooling curve with moving average and weighted moving average filtered versions, with a window length of 101	24
Figure 3.10 - Cooling curve with moving average and weighted moving average filtered versions, with a window length of 151	24

Figure 4.1 - Cooling curve generated by ALTAS displaying the 1st derivative and baseline.	27
Figure 4.2 - Close-up of Region I displaying a) cooling and 1 st , b) 2nd derivatives and ΔT curves.	30
Figure 4.3 - Close up of Region II displaying the cooling, 1st and 2nd derivative curves.	31
Figure 4.4 - 1st derivative curve showing one defined Al-Cu Eutectic peak	33
Figure 4.5 - 1st derivative curve displaying a convoluted Al-Cu peak	34
Figure 4.6 - 1st derivative curve displaying two distinct Al-Cu and AlCuMgSi eutectic peaks	34
Figure 4.7 - A part of the cooling curve showing the definition of apparent undercooling (ΔT_{α} -NUCU) and undercooling time (Δt_U)	37
Figure 5.1 - a) Unmodified silicon flakes; b) modified fibrous silicon structure 200x	41
Figure 5.2 - Section of a cooling curve displaying the depression of Al-Si eutectic temperature (dotted line represents a modified alloy)	42
Figure 5.3 - ALTAS determination of Al-Si eutectic temperature vs. Sr additions showing fading time	45
Figure 5.4 - ΔT vs. Sr additions showing corresponding AFS modification	46
Figure 5.5 - Comparison of AFS grade value vs. Sr additions for the wall and centre locations	47
Figure 5.6 - Comparison of ΔT vs. Sr additions and AFS grade value	47
Figure 6.1 - SEM micrographs (BSE mode) samples with a) 8ppm and b) 96 ppm Sr, respectively. 1 - blocky Al ₂ Cu eutectic, 2 – eutectic Al-Al ₂ Cu, 3 – fine Al ₅ Mg ₈ Cu ₂ Si eutectic types of copper phases, and 4 – iron phase.	51
Figure 6.2 - Area fraction of Cu phases as a function of Sr content	52
Figure 6.3 - Nucleation temperature of Al-Cu rich phases and solidus temperature vs. Sr content	53

Figure 7.1 - Cooling curve of 319 aluminum alloy 58

Figure 7.2 - Fraction solid as a function of temperature for the various models 61

List of Tables

Table 4.1 - Chemical composition of the ALTAS sample	26
Table 4.2 - List of Characteristic Temperatures with their corresponding symbol.	27
Table 4.3 - Definitions of the Characteristic Temperatures located in Region I	29
Table 4.4 - Definitions of all the Characteristic Temperatures located in Region II	32
Table 7.1 - Review of models for calculation of fraction solid	55
Table 7.2 - Average chemical composition of 319 aluminum alloy samples	57
Table 7.3 - Segmentation of cooling curve	57
Table 7.4 - Numerical values for f_s^{AlSi} and f_s^{AlCu} and nonlinear factors (n1, n2 and n3), for the 319 alloy.	60
Table 7.5 - A comparison of fraction solid calculated according to the present model with that of Backerud.	60
Table 7.6 - Chemical composition of the 319 aluminum alloy used in Backerud's study	61

Chapter 1. Introduction

1.1. Background

Thermal Analysis (TA) uses a cooling curve which shows a temperature drop during solidification, its time derivatives, thermodynamic descriptors and algorithms for the quantitative determination of several characteristics of the solidification process in a test sample. These characteristics can be related to the melt and consequently actual casting properties. An advanced TA system can be designed for on-line control of melt processing and prediction of the casting properties prior to the mould filling operation.

Most commercial TA systems lack the technical capabilities for comprehensive and automated assessment of the melt's metallurgical characteristics. In addition, simplification and/or analytical errors in both software and hardware design result in inherent discrepancies between TA results and the test sample structure. For example, the AluDelta TA system used for the evaluation of the AlSi eutectic temperature utilizes the reference eutectic temperature of an unmodified "generic" 319 alloy (562 ± 2.3 °C). However, this temperature depends on the melt's chemical composition, its treatment and solidification conditions. Any change in the actual versus "generic" metallurgical characteristics of the melt can result in error in the evaluation of the Si modification level.

During his work at the Industrial Research Chair (IRC), the author was responsible for the development of an advanced version of the two thermocouple TA system called the

“Aluminum Thermal Analysis System” (ALTAS). Preliminary trials have shown the technical capabilities of this system comply with Ford’s requirements, which include the following:

- automated and repeatable determination of the Al-Si eutectic growth temperature;
- robust operation of the industrial stand;
- complete documentation of test results for further analysis.

1.2. Objectives of this Work

1. To manage and contribute to the development of an advanced thermal analysis system (ALTAS) for the characterization of the 319 aluminum alloy solidification process.
2. To define characteristics and procedures used by ALTAS for the quantitative and automated analysis of the test sample solidification process.
3. To demonstrate the uses of ALTAS in metallurgical studies.

Chapter 2 Literature Review

2.1 Thermal Analysis of Binary Alloys

Thermal analysis is the study of heat evolution during the solidification process. Thermocouples placed within the molten sample as it cools monitors the temperature variations during solidification. This information is then presented as a function of time in the form of a cooling curve. The variations or deflections on the curve are created when solidification reactions take place in the cooling sample. Depending on the temperature of these deflections, it is possible to determine which particular reaction is taking place.

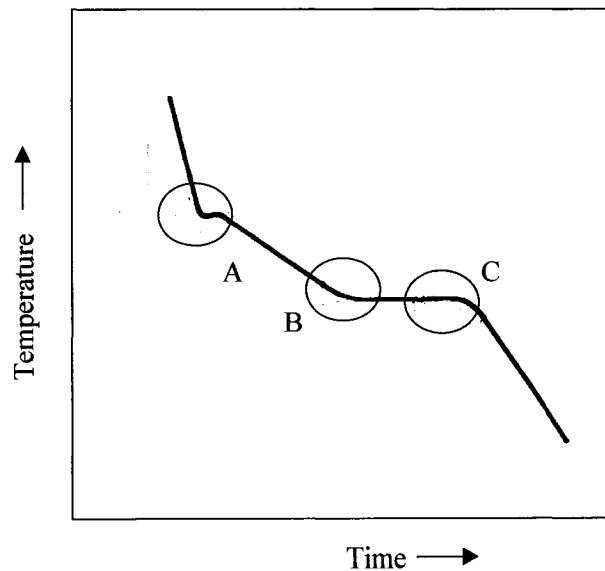


Figure 2.1 – Schematic of a cooling curve of an Al-Si binary alloy [1].

A schematic cooling curve of an Al-Si binary alloy is shown in Figure 2.1. The first deflection in the cooling curve (marked A), represents the initial nucleation of the

primary phase within the liquid metal. This point is termed the liquidus temperature and is defined as the temperature at which the primary phase crystals first nucleate. In the case of an Al-Si binary, the first phase to nucleate is α -Al dendrites. Between points A and B, the α -Al dendrites continue to grow and the solid fraction increases. At B, a eutectic transformation occurs and the Si enriched liquid phase surrounding the α -Al dendrites begins to solidify. The transformations continue in two distinct phases until the sample is solid (point C).

2.2. Binary Aluminum – Silicon Phase Diagram

Binary phase diagrams are generated through cooling curve analysis. Binary alloys of varying composition are allowed to solidify under equilibrium and arrest points are recorded and plotted on a temperature – composition diagram. Figure 2.2 displays the relationship between the cooling curve analysis and a binary phase diagram.

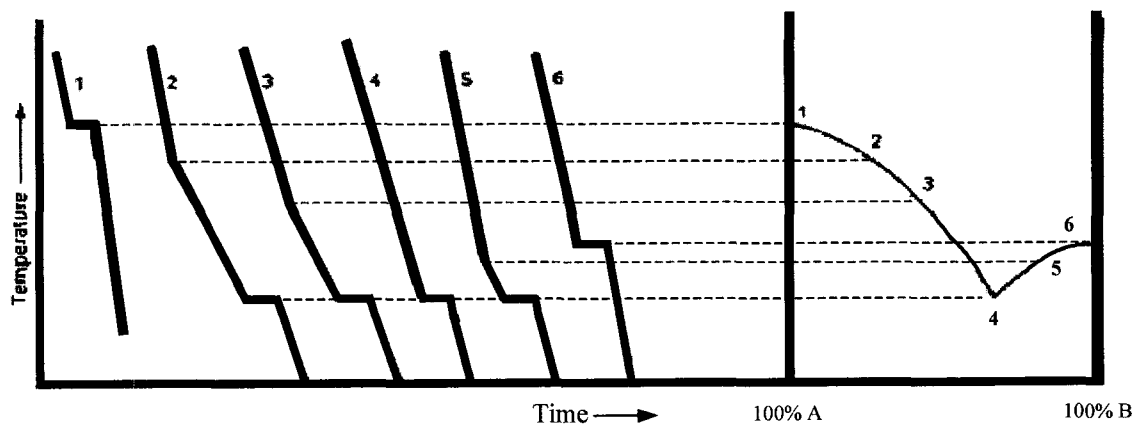


Figure 2.2 – Diagram showing how cooling curve analysis information is transferred to a phase diagram [2].

The Al-Si phase diagram is shown in Figure 2.3. The Al-Si system has a eutectic composition of 12.2% Si and a eutectic temperature of 577°C. The solubility of silicon in aluminum reaches a maximum of 1.5 at.% or 1.56 wt.% at the eutectic temperature.

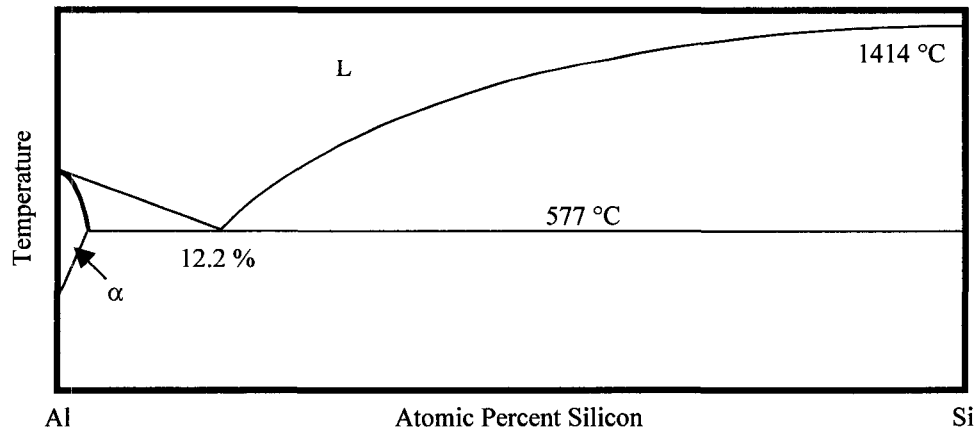


Figure 2.3 – Al-Si phase diagram [3].

Alloys with higher than eutectic additions of silicon are termed hypereutectic. In these alloys, the first phase to nucleate is the β -Si phase, which results in coarse, plate-like structures. The secondary transformation is the Al-Si eutectic structure. Hypoeutectic alloys contain silicon in amounts less than 12.2 wt%. In these alloys the first transformation is in the form of α -Al dendrites followed by the Al-Si eutectic.

2.3. Aluminum –Silicon Foundry Alloys

Binary alloys discussed in section 2.3 are not suitable for castings as they are relatively expensive and have comparatively poor properties with those that have been alloyed

further. Additions of alloying elements can significantly improve properties such as hardness, yield strength, ductility and castability among others.

In hypoeutectic Al-Si alloys (less than 12.2wt% Si) such as the 319 alloy studied in this thesis, additions of magnesium and/or copper greatly improve both the hardness and yield strength. It is the increased mechanical properties of these alloys, which make them useful in a variety of automotive and aerospace applications. In hypereutectic alloys, additions of manganese, nickel, copper and magnesium are used to increase the mechanical properties.

2.4. Review of Thermodynamics

In order to study the solidification of the 319-aluminum alloy, it is important to understand the basic thermodynamic principals that govern the transformation from a liquid phase to a solid phase. To demonstrate these thermodynamic principals we will consider a pre metallic element with only a single solid phase. Figure 2.4 displays a pressure versus temperature schematic phase diagram of a single component system. Of the three phases, solid, liquid and gas, the solid crystalline phase posses the lowest internal energy and the highest degree of order. The liquid represents a phase with slightly higher internal energy and slightly larger entropy. Finally the gas phase has the highest internal energy and the greatest entropy. The free energy curves for these three phases are drawn schematically in Figure 2.5 for each of the isobaric lines in Figure 2.4. In Figure 2.5a), it can be seen that at temperatures below the melting temperature, T_m , the

solid phase has the lowest free energy. At temperatures above T_m the liquid phase has the lowest free energy until the boiling temperature or T_b where the gas phase becomes the lowest free energy state. Figure 2.5 b) represents the free energy curves where the potential for all three phases to coexist. At the triple point temperature, T_t , all three phases are stable. Below the triple point temperature, the free energy of the solid phase is lower while above T_t , the gas phase is the most stable. Finally Figure 2.5 c) demonstrates the free energy curves at very low pressure. In this case the free energy curve of the liquid phase lies entirely above the gas phase and is never stable. In this situation the only transformation which takes place is sublimation at T_s .

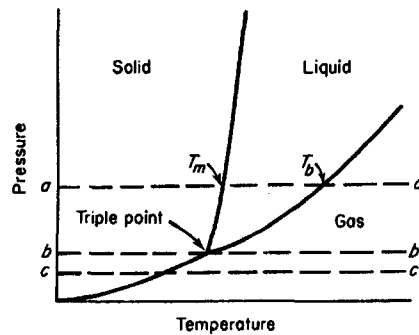


Figure 2.4 – Pressure-temperature phase diagram for a single component system including isobars [38].

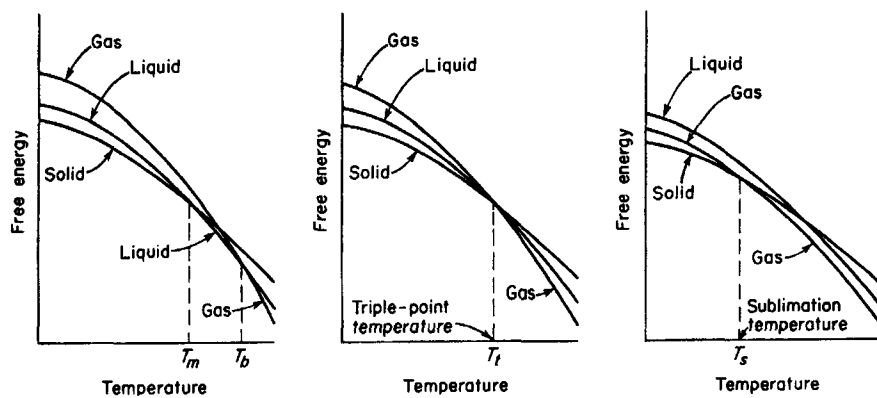


Figure 2.5 – Free energy curves for the phases in a one component system at three different pressures [38].

2.5. Nucleation

Nucleation of the solid phase within a molten metal occurs in one of two ways. The solid may form at a small foreign particle as in the case of heterogeneous nucleation. This is the mechanism that drives grain refinement discussed in Chapter 4. Conversely nucleation may result from a concentration fluctuation of the atoms or molecules as is the case for homogeneous nucleation.

Homogeneous nucleation is difficult as surface energy is generated which opposes the loss of energy as the temperature decreases. As a result, a phenomenon referred to as undercooling takes place in which the temperature continues to decrease past the melting point before the transformation of liquid to solid can take place homogeneously.

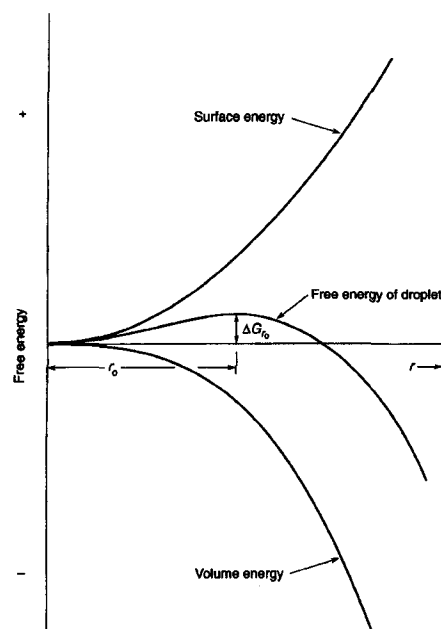


Figure 2.6 – Free energy of a particle as a function of radius [38]

Equation 2.1 represents the free energy associated with the formation of the solid particle.

$$\Delta G = \Delta G_v + \Delta G_\gamma \quad (2.1)$$

ΔG_v is the free energy associated with the volume of the particle and ΔG_γ represents the energy of the surface created. Therefore Equation 2.1 can be written as:

$$\Delta G = A_1 r^3 + A_2 r^2 \quad (2.2)$$

where A_1 and A_2 are constants and r is the particle radius. Equation 2.2 is plotted in Figure 2.6. and shows that at small radii, the surface free energy is larger than the volume free energy and the total free energy is positive. However, as the radii grows in size the free energy becomes negative. The radius at which this occurs is called the critical radius. Below the critical radius, a particle reduces its free energy by reducing in size and thus tend to disappear. Particles with radii greater then the critical radius undergo a decrease in free energy with increasing radius and are stable and tend to grow.

Equation 2.2 may also be written in the form:

$$\Delta G = 4/3\pi r^3 \Delta G_B + 4\pi r^2 \gamma \quad (2.3)$$

where ΔG_B is the chemical free energy change per atom associated with the transfer of atoms from the liquid to vapour phases divided by the volume of an atom.

By setting the derivative of Equation 2.3 to zero and solving for r_0 we obtain:

$$r_0 = -2\gamma\Delta G_B \quad (2.4)$$

Substituting Equation 2.4 back into 2.3 we obtain the free energy of the nucleus at the maximum ΔG_{r_0} .

$$\Delta G_{r_0} = 16\pi\gamma^3/3(\Delta G_B)^2 \quad (2.5)$$

In section 4.5, the effects of undercooling are discussed as to how it pertains to grain refinement and its effect on the nucleation of the aluminum dendrite formation.

Chapter 3. AITAS – Aluminum Thermal Analysis System

3.1. AITAS Hardware

For the AITAS system to be successful, the stand was designed to withstand the rigors of plant operation. To ensure the robustness of the stand, Windsor Aluminum Plant (WAP) personnel requested that Montrose Engineering complete the final design of the stand which was then manufactured at the University of Windsor's Technical Support Centre.

The stand is contained in a grounded ¼" steel cabinet to protect against high frequency noise and elevated temperatures both of which exist in close proximity to the furnace. The AITAS stand contains a locking mechanism to ensure the consistent location of the thermocouples within the thermal analysis test sample. The thermocouple assembly will be raised and lowered using a pneumatic cylinder. Since the lowering of the thermocouples introduces a pinch point, a safety cut-off is installed in order to restrict the movement of the cylinder if the cabinet door is not closed. The AITAS stand is shown in Figure 3.1.

The lowering of the thermocouple assembly results in the immersion of two thermocouple probes into the molten aluminum located in the centre and near the wall as seen in Figure 3.2. In this work, two thermocouples are required to determine the difference between the centre of the test sample and the outer wall. This information leads to the determination of the dendrite coherency temperature as defined in chapter 4.

Since the thermocouples are to be reused, it is necessary to protect the thermocouples with thin walled stainless steel sheaths.

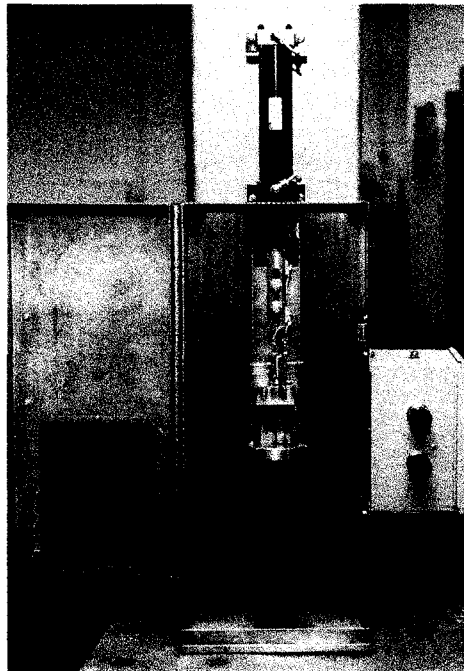


Figure 3.1 - AITAS stand

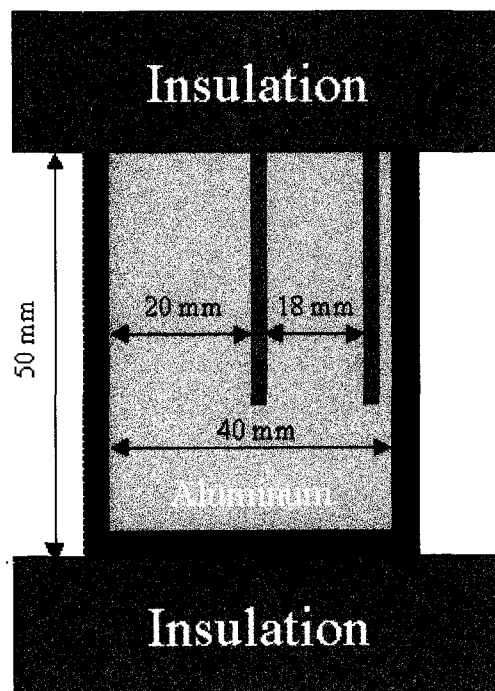


Figure 3.2 - Schematic of thermal analysis test sample (the location of the thermocouples is described in chapter 4).

A KNM-TC42-RS Smartlink Module produced by Keithley was selected for the collection of thermocouple data. The Smartlink module was selected for TA data acquisition because it is a compact “all in one” unit that is capable of performing data processing prior to delivering the information to the PC. Recently the IRC has run into several limiting features on the Smartlink module, which effect the sampling rate at high temperatures. It is therefore recommended that for future work, an alternative data logger device is acquired.

3.2. AITAS Software Capabilities

The AITAS software was programmed using labview by Jim Hochreiter of the Technical Support Centre. The AITAS system is capable of:

- Automatic detection of 11 characteristic temperatures as defined in chapter 4 (additional copper phase temperatures are left for future work, see section 4.4),
- Estimation of grain size and dendrite arm spacing,
- Measuring the depression of the Al-Si eutectic temperature due to silicon modification,
- Development of thermal analysis database which logs all relevant information.

To accommodate the various uses of the AITAS software, three different versions have been developed. Each system has additional capabilities depending on its application. These three versions include a system for "on the floor" use, a system designed for use by

supervision and finally a system to be used for research and development. Each of these systems will be described in further detail in the following sections.

3.3. AITAS System for Ford Windsor Aluminum Plant and Casting Process and Development Centre

To begin the operation of the AITAS program, the operator is required to enter a login and password. After this step, the AITAS software begins monitoring the thermocouple information in order to detect the immersion of the thermocouples into the molten aluminum. This triggers the data logging after which, the operator is given the opportunity to enter any comments that he/she may feel pertinent. When the temperature of the TA sample falls to 400°C, the AITAS program terminates the data logging and proceeds to the data processing module. Upon the completion of the data processing, three separate files are generated and saved to both the plants network drive and the computers own drive. The first of these files contains a summary of the test including all the characteristic temperatures, operator information and comments, as well as operating information such as the date, time, file name and location. The second file consists of all of the information described in the previous section, appended into an EXCEL database. This allows Ford engineers to easily plot historical information. The third file contains all the raw data for further evaluation by Ford or IRC personnel. In addition to the generation of these files, a complete summary sheet will automatically be printed. A schematic of the data flow is given in Figure 3.3. If the AITAS software is unable to process the data obtained during the test, a message is placed on the screen in order to inform the operator. In addition, a summary file will be generated with a detailed

description of the problem and will be sent to the system supervisor and printed within the melt room.

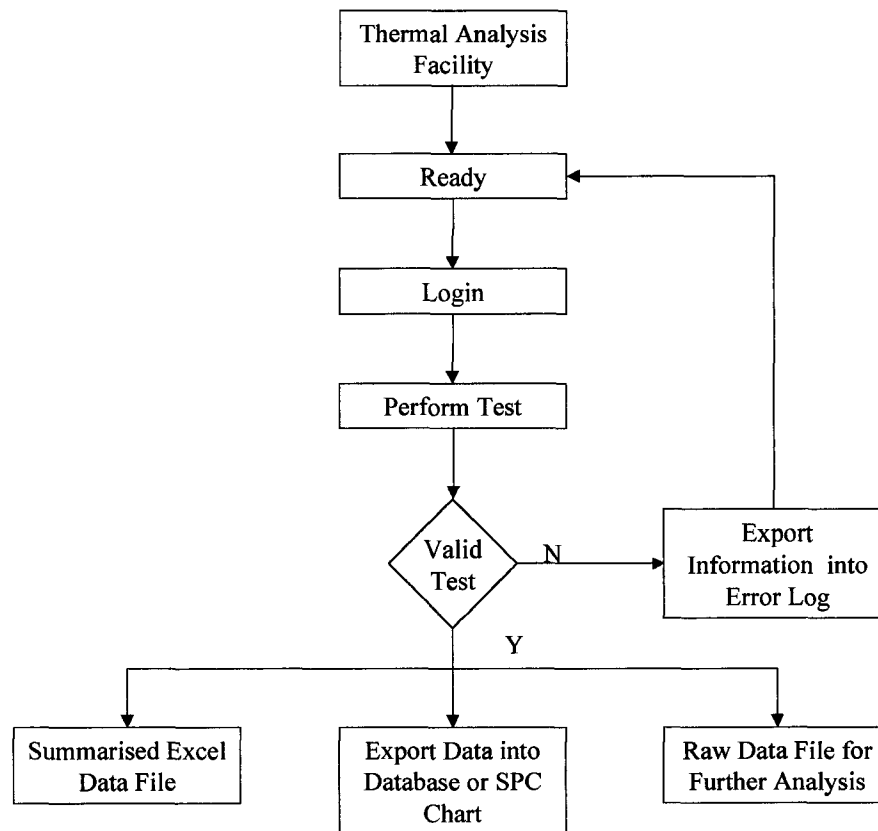


Figure 3.3 - Schematic of data flow

3.4. System for “On The Floor” Use

This system is designed to have little interaction with the operator. After the initial “logging in” process, no other input is required from the user. However, during the test, the operator is given the opportunity to insert comments. This may include apparent testing conditions that may alter the test results or special trial information, unusual melt

chemistries or casting procedures. These comments are then saved with the data.

The “On-Screen” display will advise the operator of the status of the system, as well as give all pertinent information in a simple and easily read chart. In the event of either a system or test failure, the operator will be notified and the test will be repeated.

3.5. Advanced Engineering System

This system is available to the Ford designate responsible for the system’s operation. This version of ALTAS gives the operator the opportunity to do further analysis of the thermal analysis test after entering login information. This includes concentrating on certain reactions during the solidification and obtaining time, temperature, fraction solid and cooling rate information anywhere on the cooling curve. In addition to the aforementioned capabilities, personnel may also complete detailed reports using the accompanying HiQ software.

3.6. IRC ALTAS System for the Continuous Advancement of Thermal Analysis

The IRC system is used primarily for research and development. Statistically designed experiments will be used to improve the theoretical models of the ALTAS software used to determine the grain size, dendrite arm spacing, Si modification and mechanical properties of a given test sample on a continuous basis.

In addition to the industry related applications, the ALTAS station is used to demonstrate the uses of thermal analysis in metal casting to engineering students. The system is also used extensively in lab experiments held in both the graduate and undergraduate courses offered on casting technologies.

3.7. Signal Processing

3.7.1. Introduction

Thermal analysis involves accurately identifying features in the first and second derivatives of the cooling curve. However, since a thermocouple acts as an antenna, the sampled curve contains unwanted noise, resulting in unusable first and second derivative curves. It is therefore vital that the unwanted noise is filtered from the original cooling curve in order to be able to detect variations in the derivative curves. The removal of the unwanted noise must be done in such a way as to limit the distortion of the original cooling curve as this would introduce its own error. In this study, Bessel filtering, moving average filtering and weighted moving average filtering have all been investigated, with the latter method producing the most promising results.

3.7.2. Moving Average Filtering

The derivative operation is similar to running the input through a high-pass filter. Therefore, if any derivative analysis is to be done, high frequency noise must be removed

from the original input signal in order to produce accurate and meaningful results. An optimal filter will eliminate all the noise in the signal with no distortion.

Moving average filtering is a form of non-linear filtering commonly used to smooth sets of data points. Taking the average of a moving region of the input produces the filtered signal. The middle value of this region is replaced by the average of the neighboring points. This method of noise removal takes advantage of the fact that the noise added to the system has an average value of zero, and averaging the signal out over a period of time will remove the noise.

The equation for Moving Average filtering of a discretely sampled signal is shown below [5].

$$f_{MA}(n) = \frac{1}{2M+1} \sum_{k=n-M}^{k=n+M} f(k) \quad (3.1)$$

where, f_{MA} is the moving averaged output, f is the original signal, and $2M+1$ is the length of the moving average. The moving average length is restricted to be odd because M must be a positive integer. Therefore when the moving average is taken, the center point is replaced with the average of its neighbors.

Cooling curve data was taken at 5 samples per second (5 Hz) and stored in a data file. For comparison purposes, the cooling curve is also shown filtered through a 10th order low-pass Bessel filter. The Bessel filter was used in previous versions of ALTAS and is

commonly used for noise reduction in similar applications.

Figure 3.4 shows the entire original cooling curve indicating the critical region that will be examined more closely. Figure 3.5 shows the critical region of the original curve, and an 11-point moving average filtered version. The Bessel filtered output is also shown on this plot for comparison purposes. It can be seen that the moving average filter follows the original curve much more accurately than the Bessel filtered version. The Bessel filter creates several undesirable distortions. First, the minimum and maximum temperature values are between 2 and 2.5 degrees higher in the Bessel filtered curve than in the original cooling curve. Second, the difference between the maximum and minimum points is larger than one degree in the original curve, but is only 0.5 of a degree in the Bessel filtered plot. Third, the time between the minimum and maximum points is less in the Bessel filtered curve than in the original. Since all three of these measurements are used in determining the characteristics of the casting, the Bessel filter will produce incorrect results. Although the moving average filtered versions have more noise embedded in the curve, it does not show these types of distortions.

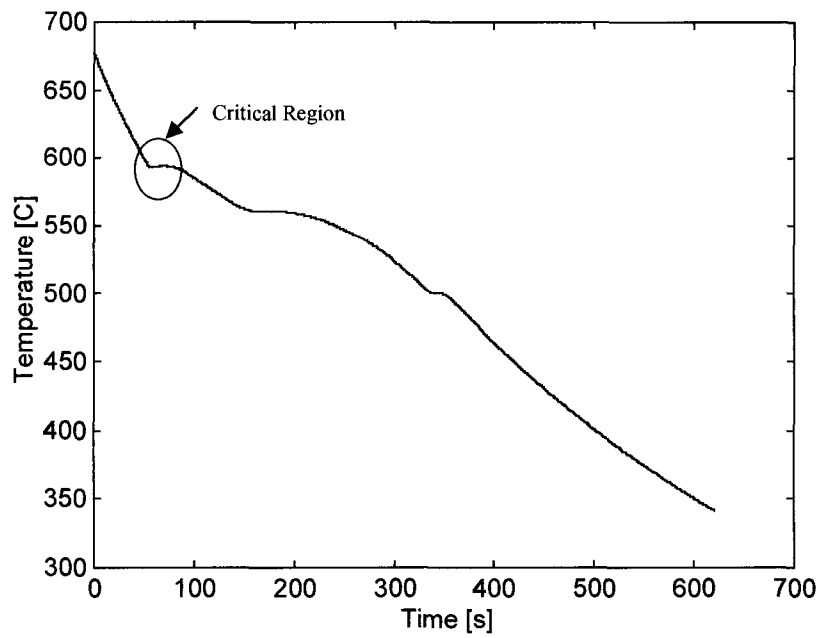


Figure 3.4 - Original cooling curve showing critical analysis.

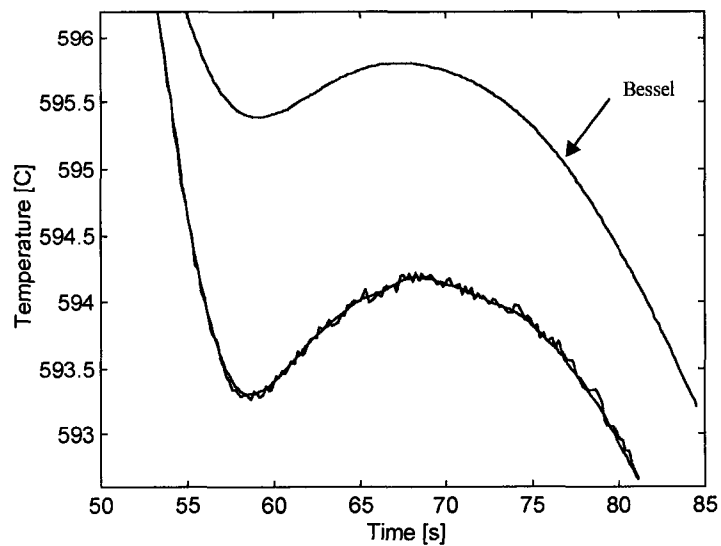


Figure 3.5 - Original curve and moving average with a window length of 11 (Bessel shown for comparison).

In Figure 3.6, the moving average length is increased to 31 points. The resulting curve has less noise, however, there is some distortion which results in a shifting of the

maximum and minimum temperatures of nearly 0.2 °C

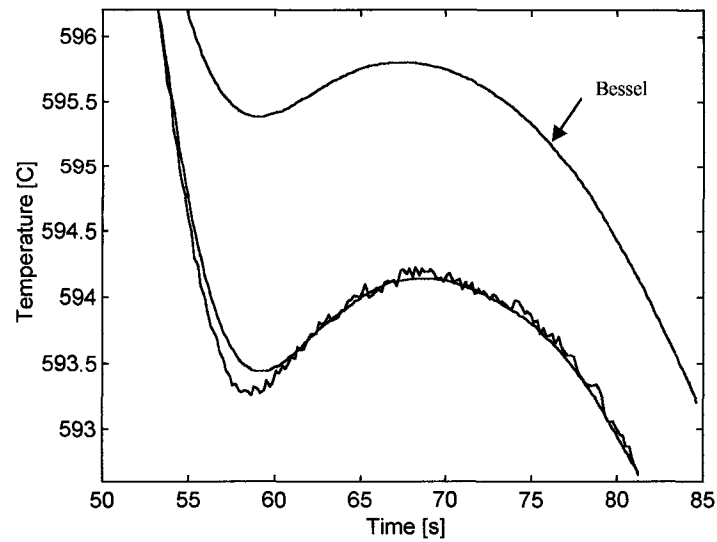


Figure 3.6 - Original curve and moving average with a window length of 31 (Bessel shown for comparison).

3.7.3. Weighted Moving Average Filtering

Although the moving average is adequate for most applications, it does not optimize the filtering of the original signal in this particular application as it assumes that the original curve is constant over the averaging length. Of course, this is not the case as the cooling curve is not simply a flat line. For the moving average filter to work well, the average length must be selected relatively small so that the original curve only changes negligibly. However, noise removal increases as the moving average length increases, so, to achieve an adequate amount of noise removal the moving average length must be increased to a length where the output is not an accurate representation of the original curve.

To solve this problem, a weighing factor or coefficient is added to each term and the method of Least Squares Linear Regression is used to choose these coefficients. Instead of using the assumption that the cooling curve is a flat line, sections of the curve can be fit to polynomials of second or third order. The equation for moving average filtering can be changed to include weight coefficients as follows [5]:

$$f_{WMA}(z) = \frac{1}{\sum_{k=z-M}^{z+M} a_k} \sum_{k=z-M}^{z+M} a_k f(k) \quad (3.2)$$

Each of the $f(k)$ values are multiplied by the weighted coefficient a_k . If these coefficients are chosen correctly, the output will produce a smoothed version of the input signal, and its first and second derivatives.

In the Figures 3.7 through 3.10, a comparison between the moving average and weighted moving average is made. The same procedure for determining the length of the window was used for the weighted moving average as was used in the previous section.

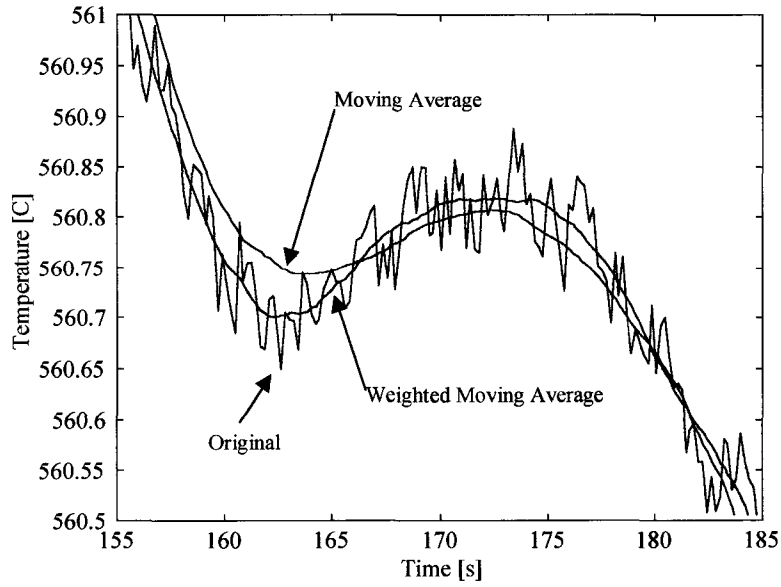


Figure 3.7 - Cooling curve with moving average and weighted moving average filtered versions, with a window length of 51.

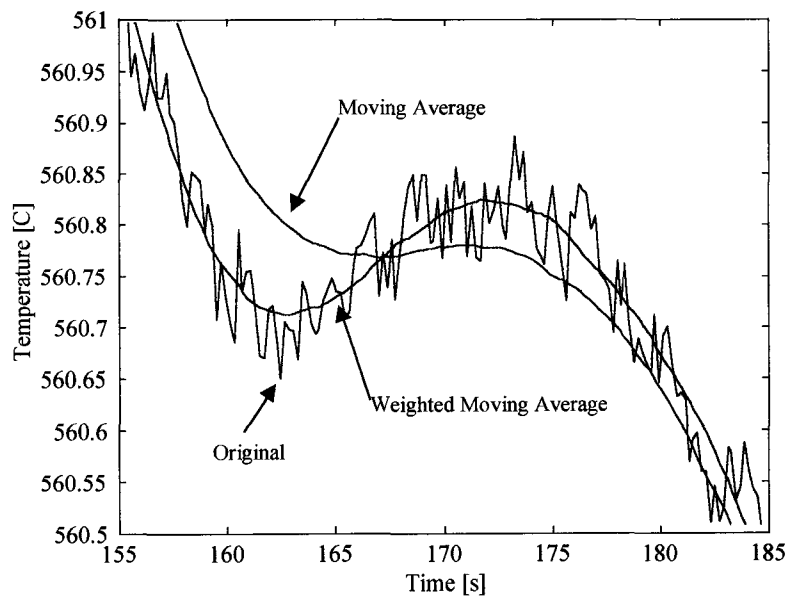


Figure 3.8 - Cooling curve with moving average and weighted moving average filtered versions, with a window length of 81.

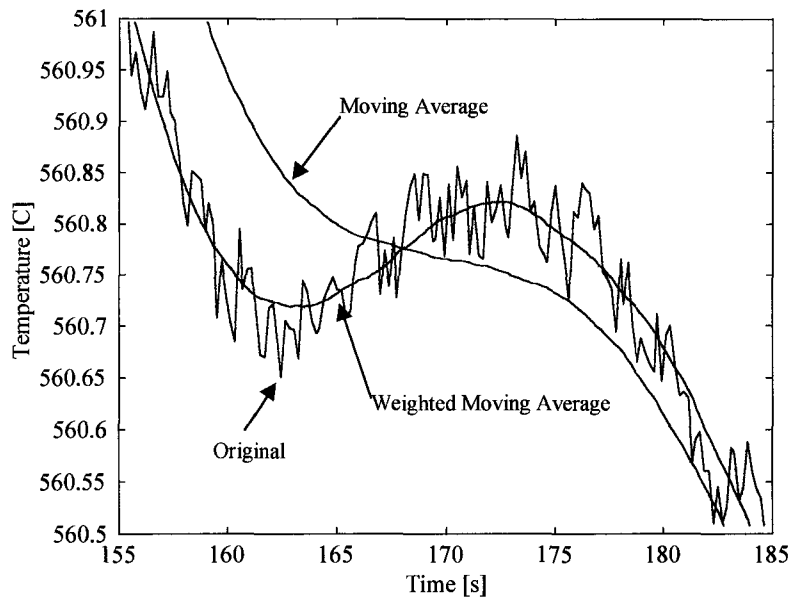


Figure 3.9 - Cooling curve with moving average and weighted moving average filtered versions, with a window length of 101.

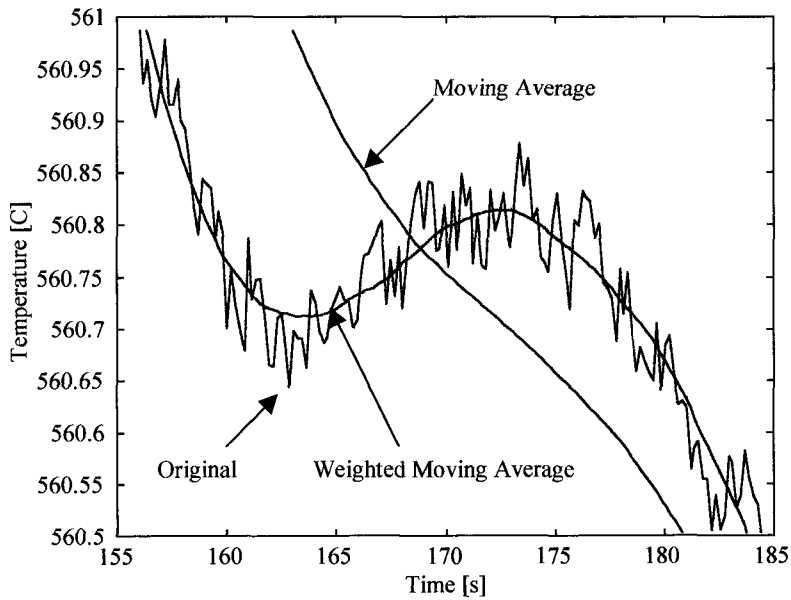


Figure 3.10 - Cooling curve with moving average and weighted moving average filtered versions, with a window length of 151.

Figure 3.7 shows the original data plotted with the moving average filtered output as well as the weighted moving average filtered output. The moving average filtered curve is

smooth, but it does not follow the original curve as closely as the weighted moving average filter output (the moving average curve shows a distortion of nearly 0.05°C). Figures 3.8 through 3.10 display the effect of increasing the width of the averaging window. In Figure 3.10 the moving average filtered output smoothes out the feature of the curve while the weighted moving average output follows it fairly closely. Therefore, it can be clearly seen that the weighted moving average produces a better approximation of the cooling curve.

3.7.4. Incorporation of Weighted Average Filtering into ALTAS

The weighted moving average filter performed on the original curve, as well as the first and second derivatives, resulted in cleaner, less noisy versions of the cooling curve and its derivatives. In addition, the weighted moving average filter resulted in the least amount of distortion from the original curve. Increasing the frequency of the data collection allows for a longer weighted moving average length window, which results in more reduction of the noise levels while reducing the distortion. However, computational time limits the length of the window. As a result, I have selected a weighted average filter with a window length of 41 was selected as an optimal filtering regime and incorporated into the ALTAS software.

Chapter 4. Analysis of Cooling Curve

4.1. Background

A cooling curve can be described as a “finger print” of the solidification process. Major and minor metallurgical reactions that are thermodynamically strong enough in terms of the latent heat evolution are manifested on the cooling curve by features such as inflection points and slope changes. Upon completion of the solidification process, the test sample structure and its properties can be related to these reactions.

An example of the AITAS generated cooling curve for the aluminum 319 alloy is presented in Figure 4.1. The chemistry can be found in Table 4.1. In order to normalize the TA test, zero time corresponds to the liquidus temperature. For the purpose of analysis, the cooling curve was divided into three regions that correspond to the formation of α -Al dendrites, Al-Si eutectic and Cu rich eutectic(s) respectively.

Table 4.1 – Chemical Composition of the AITAS Test Sample (wt%) [15].

Si	Fe	Cu	Mn	Mg	Ni	Zn	Ti	Sb	P	Na
7.55	0.39	3.45	0.24	0.33	0.008	0.009	0.122	0.052	0.0015	0.0004

Computer aided analysis of the cooling curve requires utilization of unbiased procedures for statistically precise and accurate detection and evaluation of these characteristic points and regions on the curve. In order to reveal the temperature and time, as well as more complex relationships, the first time derivative (dT/dt) is used in Figure 4.1. Characteristics of the cooling curve from Figure 4.1 are summarized in Table 4.2.

Table 4.2 - List of Characteristic Temperatures with their corresponding symbol.

	Description	Symbol
1.	α -Al dendrite nucleation (liquidus) temperature	$T^{\alpha, DEN}_{NUC}$
2.	α - Al dendrite undercooling temperature	$T^{\alpha, DEN}_{MIN}$
3.	α -Al dendrite growth (recalescence) temperature	$T^{\alpha, DEN}_G$
4.	α -Al dendrite coherency point	$T^{\alpha, DEN}_{COH}$
5.	Al-Si eutectic nucleation temperature	$T^{Al-Si}_{E,NUC}$
6.	Al-Si eutectic minimum temperature	$T^{Al-Si}_{E,MIN}$
7.	Al-Si eutectic growth temperature	$T^{Al-Si}_{E,G}$
8.	Cu rich eutectic nucleation temperature	$T^{Cu}_{E,NUC}$
9.	Cu rich eutectic minimum temperature	$T^{Cu}_{E,MIN}$
10.	Cu rich eutectic growth temperature	$T^{Cu}_{E,G}$
11.	End of solidification process (solidus temperature)	T_{END}

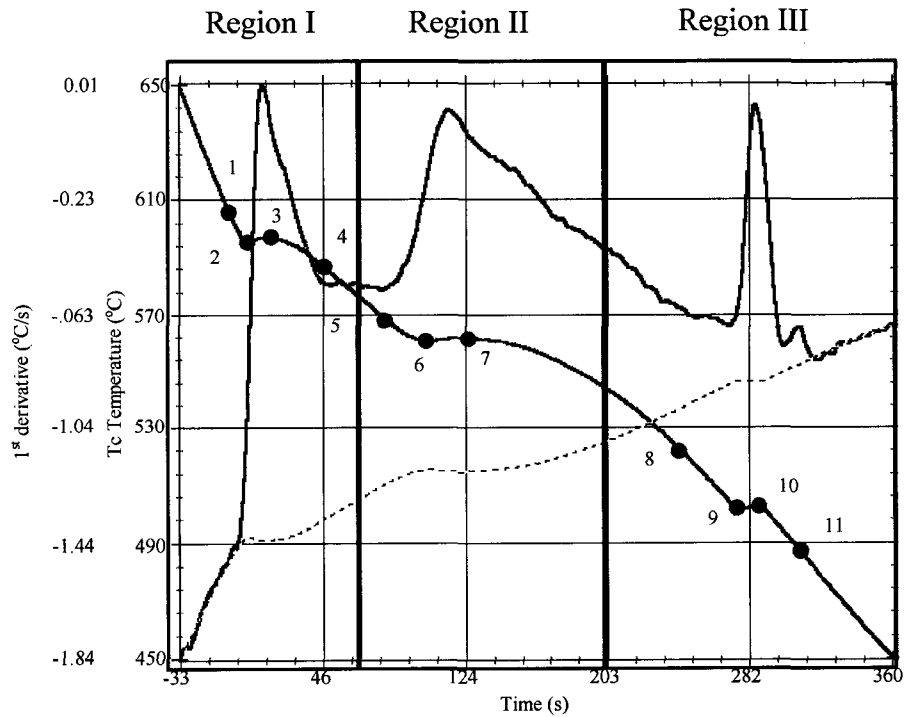


Figure 4.1 - Cooling curve (in red) generated by AITAS displaying the 1st derivative (in black) and the baseline(dotted line).

It was shown by Zindel et al. [13] and Backerud et al. [24] that the temperatures in Table 4.2 and shown in Figure 4.1 correspond to the metallurgical reaction discussed in Tables 4.3 and 4.4.

Based on Figure 4.1 the metallurgical reactions for the Fe and Mg rich phases were not observed as distinct peaks on the first derivative. Recent work at the University of Montreal [4] revealed that the Fe phase can only be detected for iron levels higher than 0.7 wt %. In the 319 alloy a small amount of Mg is often present in the form of a eutectic together with Cu. This is manifested as a convoluted (overlapped) first derivative peak in region III.

4.2. Region I - Liquidus and Dendrite Coherency

In Figure 4.1, Region I, four (4) distinct parameters (features) of the cooling curve can be distinguished by using the first and second derivatives. A close-up of this region, Figure 4.2, depicts these features while Table 4.3 summarizes their definitions. Based on these measurements and calculations, the grain size and grain refinement can be quantified.

Table 4.3 - Definitions of the Characteristic Temperatures located in Region I

Symbol	Name	Detection Algorithm	Definition
$T^{\alpha\text{DEN}}_{\text{NUC}}$	α -Al dendrite nucleation temperature (Liquidus)	This is point 1 on the second derivative curve projected to the cooling curve. (See Figure 4.2). This corresponds to the intersection of the zero axis with the line projected from the liquidus peak ($dT^2/dt^2=0$).	This is the point at which primary α -Al dendrites begin to solidify from the melt.
$T^{\alpha\text{DEN}}_{\text{MIN}}$	α -Al dendrite undercooling temperature.	This is point 2 on the first derivative and is projected to the cooling curve. (See Figure 4.2). This represents a local minimum temperature on the cooling curve. It is determined as the point at which the first derivative intersects the zero line ($dT/dt=0$).	At this point, the nucleated dendrites have grown to such an extent that the latent heat liberated balances the heat extracted from the sample. After this point the temperature of the melt increases to the steady state growth temperature.
$T^{\alpha\text{DEN}}_{\text{G}}$	α -Al dendrite growth temperature (recalescence)	This is point 3 on the first derivative projected to the cooling curve. (See Figure 4.2). This temperature follows undercooling and represents a local maximum on the cooling curve. It corresponds to the second zero point on the first derivative curve following the start of nucleation ($dT/dt=0$).	If the first derivative curve in this region does not intersect the zero line, $T^{\alpha\text{DEN}}_{\text{MIN}}$ and $T^{\alpha\text{DEN}}_{\text{G}}$ temperatures are identical and correspond to the maximum point on the first derivative curve.
$\Delta T^{\alpha\text{-NUC}}_{\text{U}}$	Depression of α -Al dendrite growth temperature	$\Delta T^{\alpha\text{-NUC}}_{\text{U}}$ can be expressed by equation: $\Delta T^{\alpha\text{-NUC}}_{\text{U}} = T^{\alpha\text{-NUC}}_{\text{G}} - T^{\alpha\text{-NUC}}_{\text{MIN}}(1)$	
$T^{\alpha\text{DEN}}_{\text{COH}}$	Dendrite coherency point	This is point 4 on the ΔT curve. (See Figure 4.2). ΔT (point 4) represents the largest difference between T_{W} and T_{C} (the wall and centre temperature). This point can be detected by using the two-thermocouple technique.	Metallurgically, the dendrite coherency point defines the temperature at which a skeleton network of dendrites have formed from the casting wall to the centre of the casting.

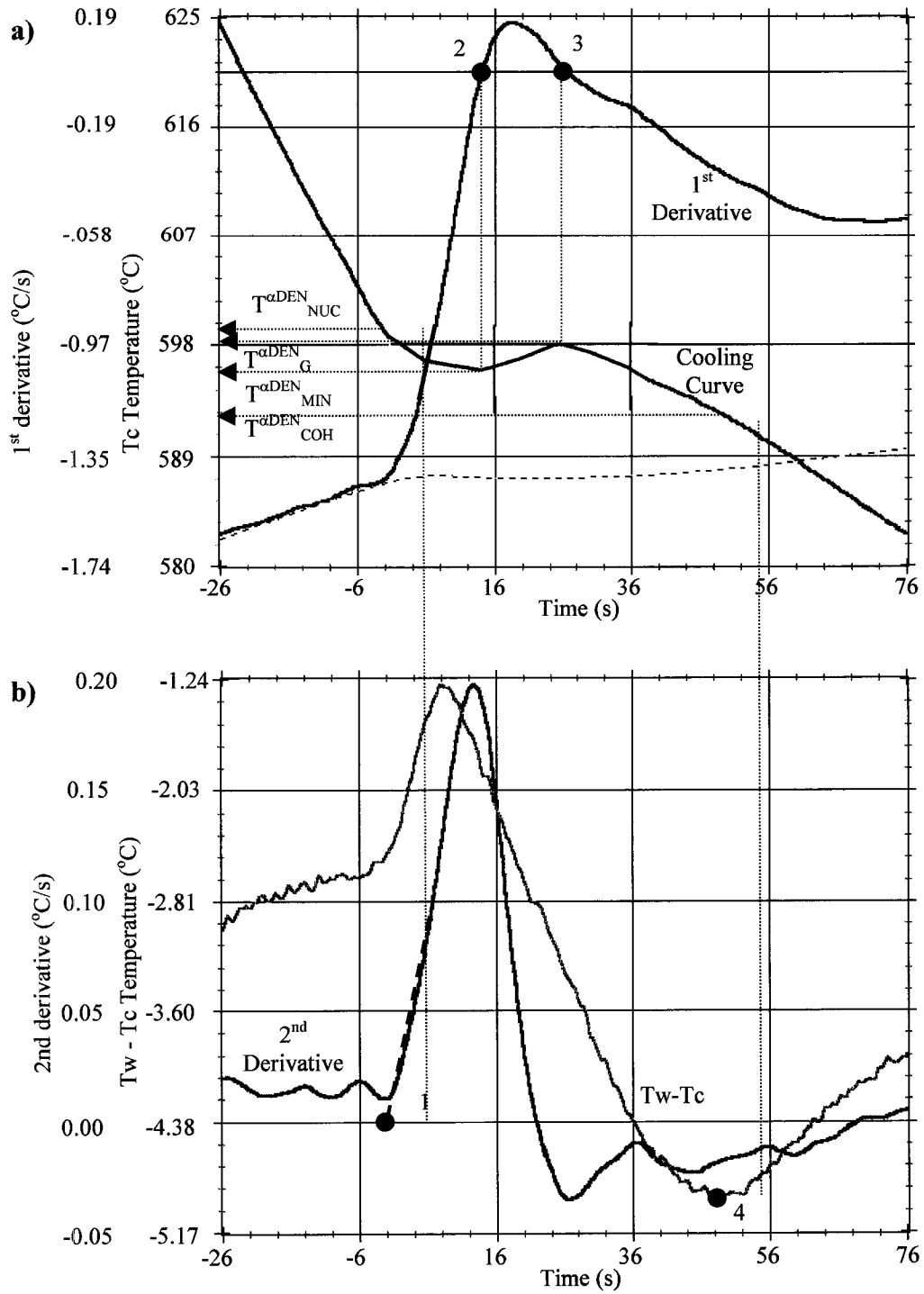


Figure 4.2 - Close-up of Region I displaying a) cooling and 1st, b) 2nd derivatives and ΔT curves.

4.3. Region II - Al-Si Eutectic

In Al-Si-Cu alloys, silicon modification exerts the most significant effect on the Al-Si eutectic reaction. In order to quantify the Si modification levels it is necessary to analyze and compare modified and unmodified cooling curve parameters. A close-up of this region, Figure 4.3, depicts these features while Table 4.4 summarizes their definitions.

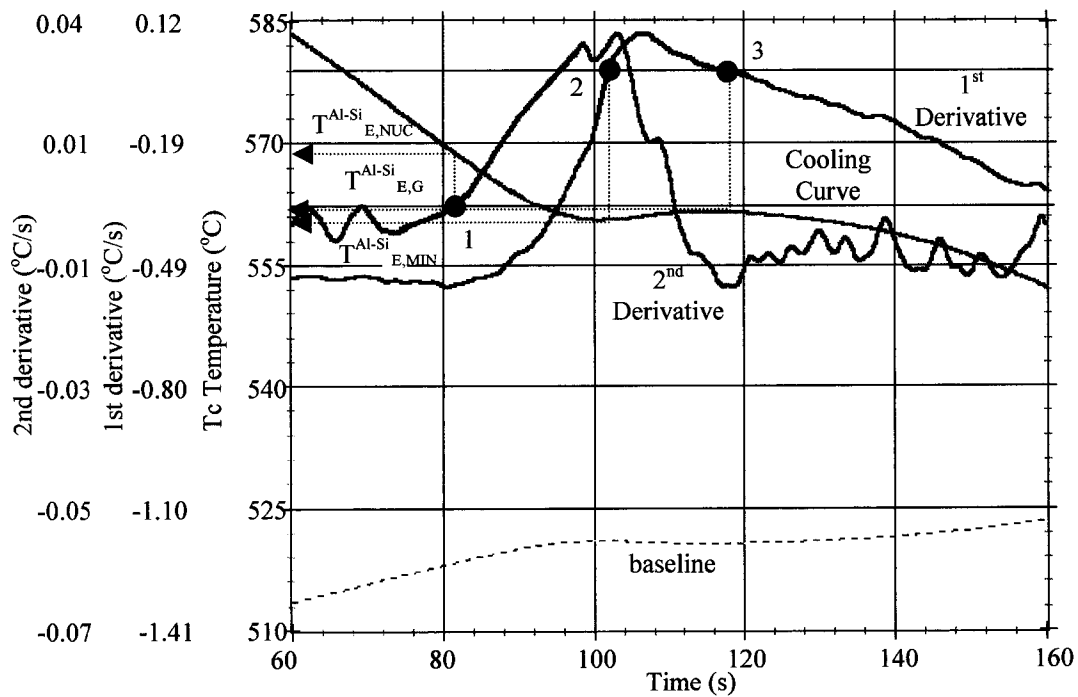


Figure 4.3 - Close up of Region II displaying the cooling, 1st and 2nd derivative curves.

Table 4.4 - Definitions of all the Characteristic Temperatures located in Region II

<u>Symbol</u>	<u>Name</u>	<u>Algorithm used for Detection</u>	<u>Definition</u>
$T_{E,NUC}^{Al-Si}$	Al-Si eutectic nucleation temperature.	This is point 5 on the second derivative and is projected onto the cooling curve. (See Figure 4.3). This corresponds to the intersection of the second derivative and the zero axis prior to the Al-Si eutectic peak ($dT^2/dt^2 > 0$).	This is the temperature at which silicon particles begin to nucleate, forming Al-Si eutectic.
$T_{E,MIN}^{Al-Si}$	Al-Si minimum eutectic temperature	This is point 6 on the first derivative. (See Figure 4.3). This temperature represents a local minimum on the cooling curve and is defined as the point at which the first derivative intersects the zero line following the Al-Si nucleation temperature ($dT/dt=0$).	Metallurgically, this temperature represents the first point at which the latent heat generated due to eutectic growth equals the heat loss from the test sample.
$T_{E,G}^{Al-Si}$	Al-Si eutectic growth temperature (sometimes referred to as the eutectic plateau temperature).	This is point 7 on the first derivative. (See Figure 4.3). This point corresponds to a second zero point on the first derivative curve following the Al-Si nucleation temperature ($dT/dt=0$).	Metallurgically, this point represents the temperature at which considerable eutectic growth occurs. If the first derivative curve does not intersect the zero line, $T_{E,MIN}^{Al-Si}$ and $T_{E,G}^{Al-Si}$ temperatures are identical and correspond to the maximum point on the first derivative curve.
$\Delta T_{E,G}^{Al-Si}$	Depression of Si eutectic growth temperature (both modified and unmodified).	$\Delta T_{E,G}^{Al-Si}$ can be expressed by equation: $\Delta T_{E,G}^{Al-Si} = T_{E}^{Al-Si} - T_{E,MIN}^{Al-Si}$	
$\Delta T_{E,GMOD}^{Al-Si}$	The level of Si modification	$\Delta T_{E,GMOD}^{Al-Si}$ can be expressed by equation: $\Delta T_{E,MODIFICATION}^{Al-Si} = T_{E,UNMODIFIED}^{Al-Si} - T_{E,MODIFIED}^{Al-Si}$	

4.4. Region III – Low Melting Temperature of Al_2Cu and Al-Cu-Si-Mg Eutectic Reactions and the End of the Solidification Process

Depending on the melt chemical composition, the cooling rate and liquid metal processing, up to three copper rich phases can be present in the test sample. Preliminary metallographic analysis revealed the presence of Al_2Cu phases in the form of blocky coarse particles and fine eutectic. In addition, an Al-Mg-Cu-Si phase was identified. At the present time the distinct and/or convoluted peaks of the first derivative of the cooling curve can detect the combination of these phases. The following Figures (4.4 to 4.6) depict three possible cases. Metallographic and convolution analysis for the eutectic characteristic temperatures will be left for future work.

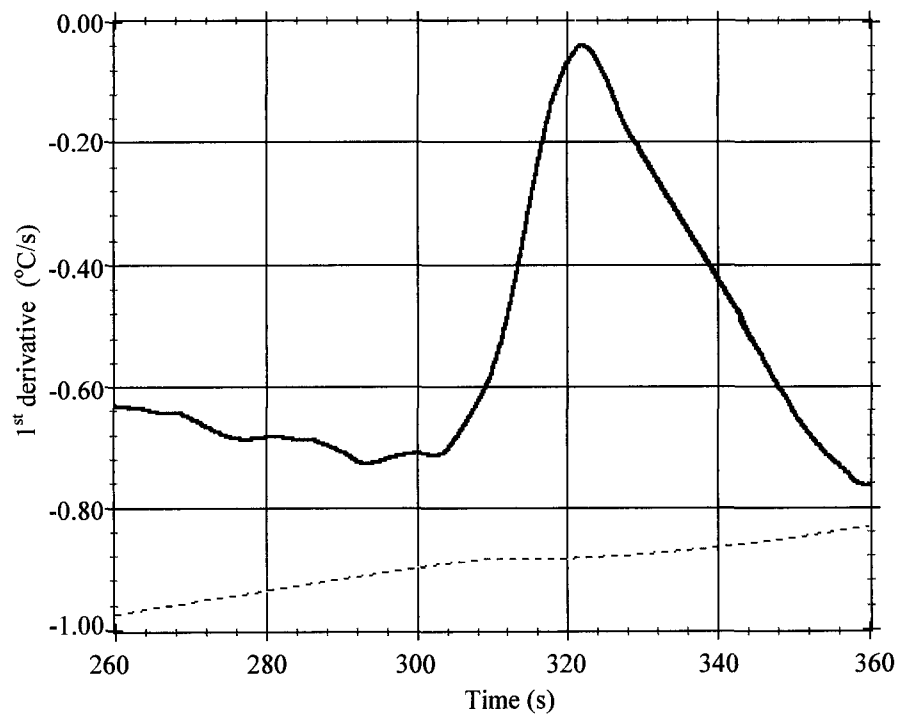


Figure 4.4 - 1st derivative curve showing one defined Al-Cu eutectic peak

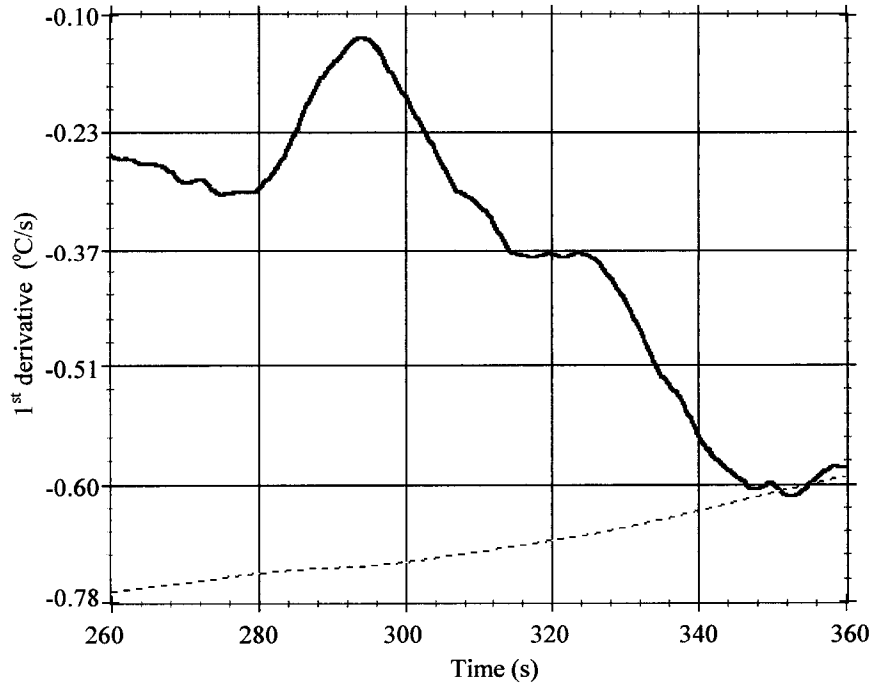


Figure 4.5 - 1st derivative curve displaying a convoluted Al-Cu peak

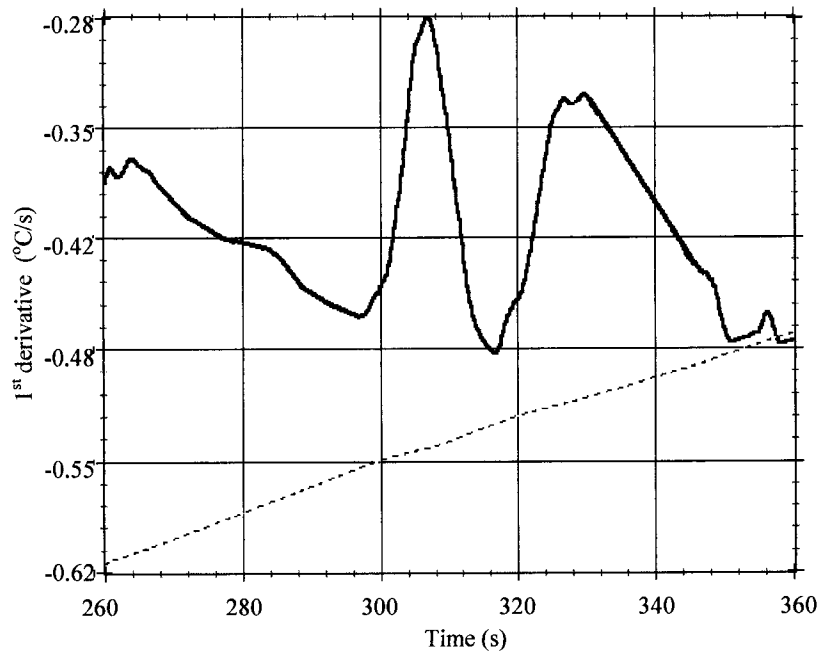


Figure 4.6 - 1st derivative curve displaying two distinct Al-Cu and AlCuMgSi eutectic peaks

4.5. Determination of Grain Size

4.5.1. Literature Search

A uniform dispersion of fine grains results in castings that have better mechanical and physical properties. According to the literature [6], there are four possible methods to achieve grain refinement:

- Addition of nucleation agents
- Forced convection
- Varying the solidification parameters
- Ultrasound treatment

According to McCartney[7] as well as Sigworth and Whalen [8] grain refinement is used to achieve:

- Better mechanical properties (ex. yield and tensile strength, elongation, hardness)
- Better product surface
- Reduced homogenization time
- Improved distribution of second phase particles and microporosity on a fine scale
- Improved machineability
- Better feeding in order to reduce shrinkage
- Reduced tendency of hot tearing

Cooling curves have been used to study grain refinement as the shape of the cooling curve at the beginning of dendrite solidification yields information on grain size. The determination of the most important relations in the primary Al regime for the 319 Al-alloy of the cooling curve are schematically illustrated in Figure 4.7.

Grain refinement occurring during solidification can be indicated as a function of undercooling magnitude and undercooling time occurring during liquidus arrest. The shape of the cooling curve at the very beginning of the solidification process gives a good indication of the number of nuclei present in the melt. When there is a great number of nuclei, the shape of the curve exhibits little undercooling (as illustrated in Figure 4.8 by the dotted line). When there are few nuclei, there is more undercooling (which is illustrated in the Figure 4.8 by the solid line).

The relationship between $T^{\alpha, \text{DEN}}_{\text{MIN}}$ and $T^{\alpha, \text{DEN}}_{\text{G}}$, is mathematically expressed by equation (4.1). This equation can be used as a criterion for the estimation of grain size.

$$\Delta T^{\alpha, \text{-NUC}}_{\text{U}} = T^{\alpha, \text{DEN}}_{\text{G}} - T^{\alpha, \text{DEN}}_{\text{MIN}} \quad (^\circ\text{C}) \quad (4.1)$$

The undercooling duration (Δt_{U}), can also be used for the determination of the grain size (i.e. the larger Δt_{U} , the coarser the grain). The duration may be defined as the time between the minimum and maximum on the cooling curve in Figure 4.7 and can be mathematically expressed by the following:

$$\Delta t_U = t^{\alpha, DEN}_G - t^{\alpha, DEN}_{MIN} \quad (4.2)$$

The duration may be also distinguished by the time running between several characteristic points in the region under consideration. Some authors [8], recognize two undercooling intervals, (t_1 and t_2). The undercooling arrest time t_1 is the time interval between the $T^{\alpha, DEN}_{NUC}$ and $T^{\alpha, DEN}_{MIN}$. The undercooling arrest time t_2 is the time interval between $T^{\alpha, DEN}_{NUC}$ and $T^{\alpha, DEN}_G$.

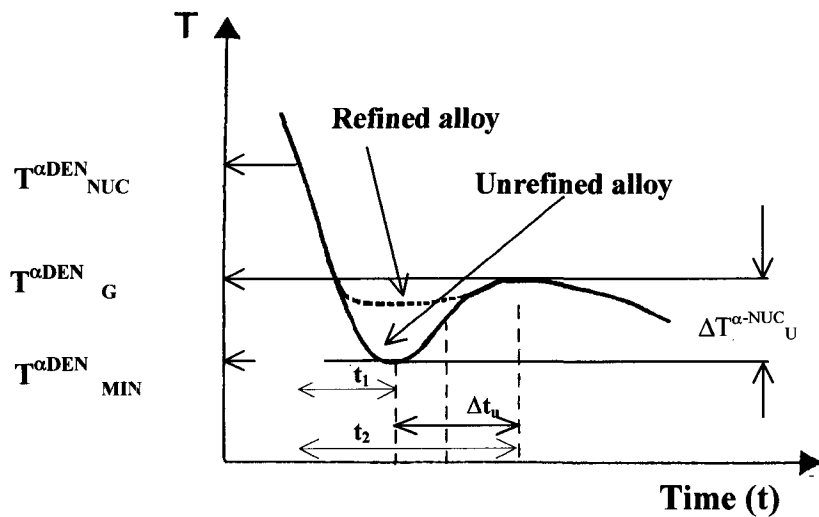


Figure 4.7 - A part of the cooling curve showing the definition of apparent undercooling ($\Delta T^{\alpha-NUC}_U$) and undercooling time (Δt_U).

In recent literature, several models have been proposed for the assessment of grain size using thermal analysis. Based on laboratory experiments, Chai [9] developed an equation which related the grain size (radius, R_f) with the average dendritic growth rate (V_a) and the solidification time at the dendrite coherency point (t^*):

$$R_f = V_a t^* \quad (4.3)$$

Thus, grain size can be estimated using the following equation:

$$R_f = A t^* / (0.86\Delta T^* + 316 (f_s^*)^2) \quad (4.4)$$

Where A is the constant and ΔT^* is the temperature difference between the nucleation of α -Al crystals and the dendrite coherency point. However, verification of this model revealed a considerable discrepancy between the TA results and metallographically measured grain size.

An equation was developed which relates grain size (GS) with characteristic points on the thermal cooling curve ($t^{\alpha, DEN}_G$ and $t^{\alpha, DEN}_{NUC}$) for Al-Si-Cu alloys. The calculated value of GS is expressed in terms of an ASTM scale value (from 1 to 14).

$$GS = A_0 + A_1 F \quad (4.5)$$

Where:

$$A_0 = 14.39$$

$$A_1 = -0.36$$

$$F = t^{\alpha, DEN}_G - t^{\alpha, DEN}_{NUC}$$

The constants A_0 and A_1 in equation (4.5) were determined by linear regression analysis, while the variable F represented the time difference between two characteristic points on the cooling curve (expressed in seconds).

Ananthanarayanan et al. [10], investigated the influence of the cooling rate on the grain size in the 319 aluminum alloy. Based on their work, the IRC Team has developed an equation, which describes the change in the grain size in relation to the average cooling rate:

$$GS = 10^{[3.1347 - 0.1985(\log R)]} \quad (4.6)$$

Where (R) is the average cooling rate determined by dividing the temperature interval between liquidus and solidus by the respective time intervals.

Equations 4.1 through 4.4 are related to the grain size before refinement and are a function of different cooling rates. Analysis of the average cooling rate, which has been done on the first derivative of the 319 Al-alloy cooling curve, shows that the cooling rate for the temperature solidification interval of the 319 alloy is practically constant (0.37°C/s). Therefore, a new experimental investigation needs to be done in which the influence of melt chemistry and melt processing on the grain size will be included.

4.5.2. AITAS Determination of Grain Size Refinement

Currently, the author has chosen to use Equation 4.6, due to the fact that it pertains specifically to the 319-aluminum alloy, whereas the other models have been developed using the 356-aluminum alloy. The author recommends that further metallographic verification be performed and corrections made if need be.

Chapter 5. The Effect of Strontium on Aluminum – Silicon Modification

5.1. Silicon Modification Literature Search

In Al-Si foundry alloys, silicon crystals in the eutectic mixture normally grow in a faceted manner, which results in poor mechanical properties (see Figure 5.1a). The commercial application of these alloys often depends on the modification of the eutectic silicon crystals. This is performed by additions of strontium [11] or sodium of low concentrations, which induce twinning in the growth of the silicon crystal. This twinning results in a fine fibrous structure shown in Figure 5.1b.

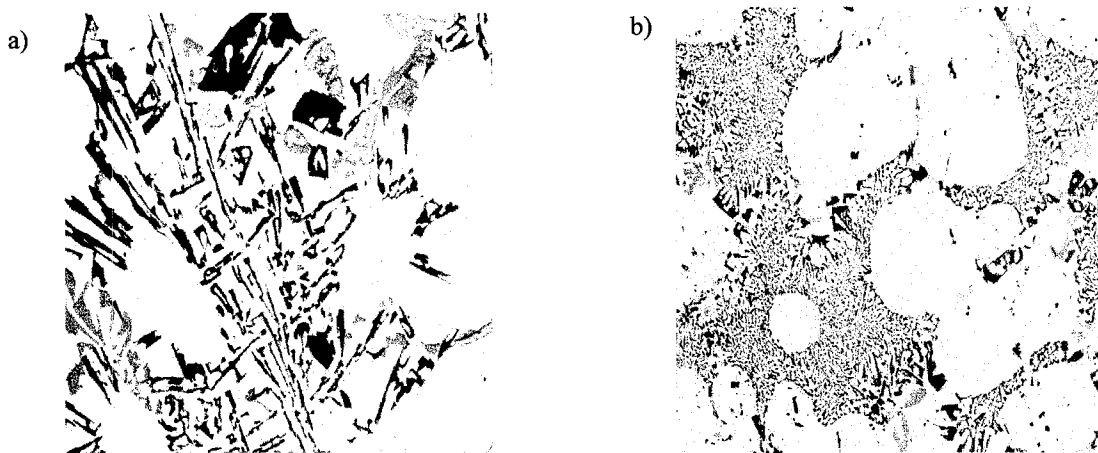


Figure 5.1 – a) Unmodified silicon flakes; b) modified fibrous silicon structure (200X) [12].

The additions of these elements cause changes primarily in the nucleation and growth mechanisms of the eutectic silicon phase [13]. This reflects on the final mechanical properties of the aluminum-silicon alloy. For instance, it can improve tensile elongation, machinability and alter the casting characteristics.

Figure 5.2 shows the effect of Si modification on the cooling curves for the Al-Si eutectic reaction. Modified eutectic solidification occurs at a nearly constant temperature, which is about 8-10°C below the unmodified equilibrium eutectic temperature (for the 319 Al-Si alloy the equilibrium eutectic temperature is about 562°C). Both the nucleation and growth eutectic temperatures are depressed by the addition of modifiers. See Figure 5.1, [14]. The amount of the depression ($\Delta T_{E,G}^{Al-Si}$), has been correlated with the degree of modification [15-17]. The greater the ΔT value, the more complete the modification is. Some authors suggest that the cooling rate [18] should be included together with ΔT to estimate the degree of modification.

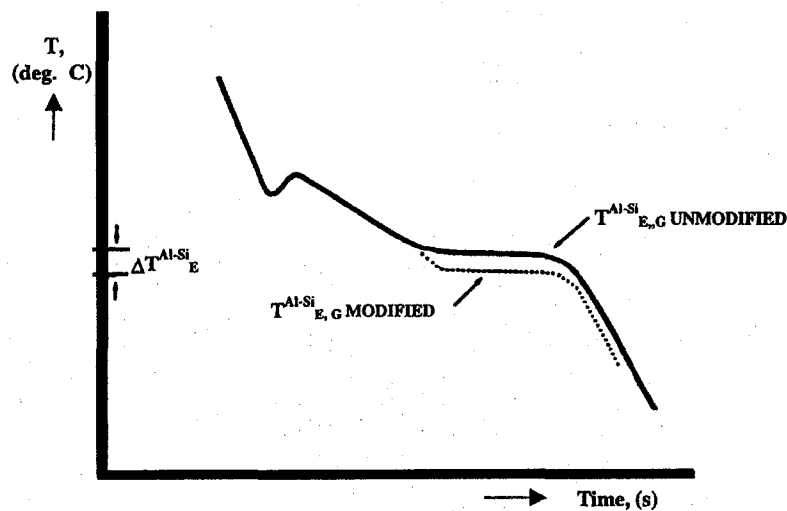


Figure 5.2 – Section of a cooling curve displaying the depression of Al-Si Eutectic Temperature (Dotted line represents a modified alloy) [19].

5.2. AITAS Determination of Silicon Modification

Currently the AITAS system is using the same procedure as the current system in place at the Windsor Aluminum Plant, AluDelta. The procedure has been previously explained in Section 4.3 and is described by equation 5.1.

$$\Delta T_{E,G,MOD}^{Al-Si} = T_{E,UNMODIFIED}^{Al-Si} - T_{E,MODIFIED}^{Al-Si} \quad (5.1)$$

5.3. Experimental Work

Following is a portion of the work completed by the author in collaboration with Dr. M. Djurdjevic under the supervision of Dr. J. Sokolowski. This work looked at the effect of strontium on the copper eutectic as contained in the paper entitled “The Effect of Strontium on the Microstructure of the Aluminum-Silicon and Aluminum Copper Eutectics in the 319 Aluminum Alloy”.

5.3.1. Objectives

1. To Quantify the relationship between AITAS cooling curve characteristics, pertaining to the AlSi eutectic region with the Sr level and its fading behaviour, using WAP ingots remelted in the IRC laboratory
2. To compare the visually determined Si modification level (based on the AFS chart) with Sr content and AITAS measurements

3. To establish a quantitative relationship between Sr level, ΔT and the AlSi eutectic modification level in ALTAS laboratory test samples, with identical chemical compositions, at two different locations of the test sample

5.3.2. Experimental Procedure

WAP 319 aluminum alloy ingots produced by Alchem were used in this experiment. The ingots were melted in an electric resistance furnace and kept at a temperature of 730 ± 5 °C. The melt was degassed for 15 minutes using an argon lance, however, no protective atmosphere was utilized during melt holding. It was then modified through the addition of 10% Sr master alloy. An incubation time of 15 minutes was allowed prior to collecting the first sample. These samples were then taken by submerging a cylindrical graphite cup (40mm in diameter, 50mm deep) into the melt.

In order to study the fading effect of Sr over time, four samples were taken in 12 minute intervals before the next Sr additions was made. Changes in the AlSi eutectic growth temperature ($T_{E,G}^{Al-Si}$) as a function of the Sr level, were determined using ALTAS cooling curves.

The level of Si modification ($T_{E,G,MOD}^{AL-Si}$) was determined according to the following formula of Equation 5.1. Light optical microscopy specimens were cut from the test samples close to the tips of the thermocouples.

5.3.3. Results

Figure 5.3 shows that the addition of Sr increases the ΔT modification. When the Sr level is increased from 8 to 96 ppm the ΔT modification increases to a maximum of approximately 12 °C for those samples taken 15 minutes after the Sr addition. In other words, Sr addition increases the level of modification.

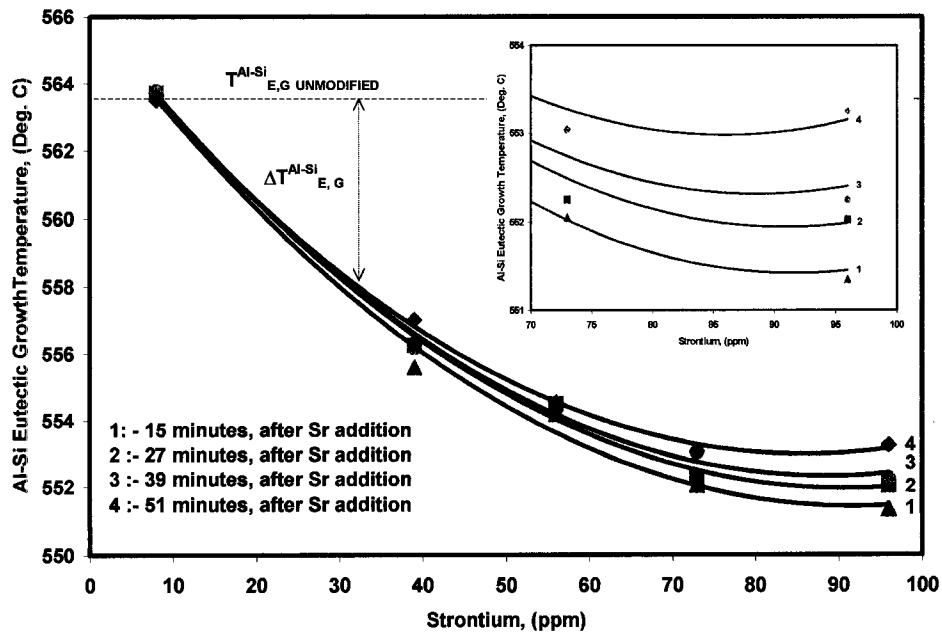


Figure 5.3 – ALTAS determination of Al-Si eutectic temperature vs. Sr additions showing fading times [12].

Figure 5.3 also shows that the longer holding times (up to 51 minutes) decrease the ΔT modification by up to 2°C in high Sr samples.

Figure 5.4 depicts the relationship between Sr level, ΔT modification and the resulting Si modification level (according to AFS chart). Increasing Sr corresponds with a higher ΔT modification and degree of Si modification. A Si modification level of #1-3 was

obtained for a Sr concentration between 8 and approximately 60 ppm. The addition of Sr to a level of approximately 70 ppm produced a modified eutectic structure #4. Further addition of Sr to 96 ppm produced the finer fibrous AlSi eutectic structure #5.

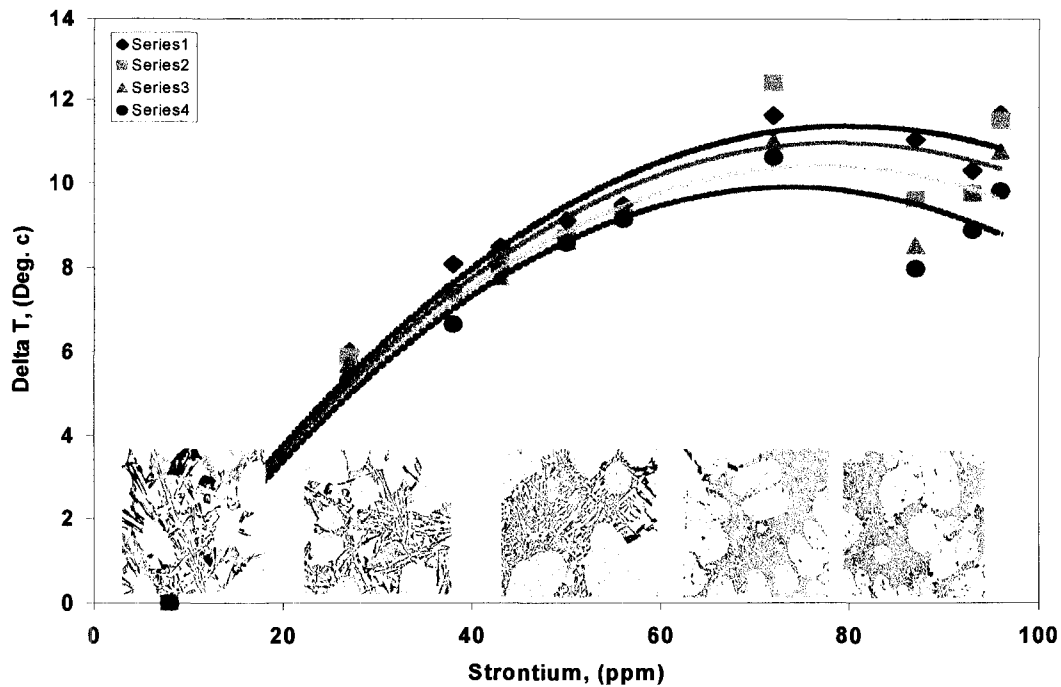


Figure 5.4 – ΔT vs. Sr addition showing the corresponding AFS modification [12].

Metallographic observation revealed that Sr effects the characteristics of Cu rich phases (type and volume fraction) and porosity.

Figure 5.5 shows the relationship between the AFS Grade (i.e. AlSi eutectic modification level) and the Sr level at two different locations on the ALTAS test samples. The slightly higher solidification rates at the radius of the wall thermocouple had little effect on AFS grade. Therefore, all subsequent analyses are based on the average of the measurements taken at the wall and centre thermocouples.

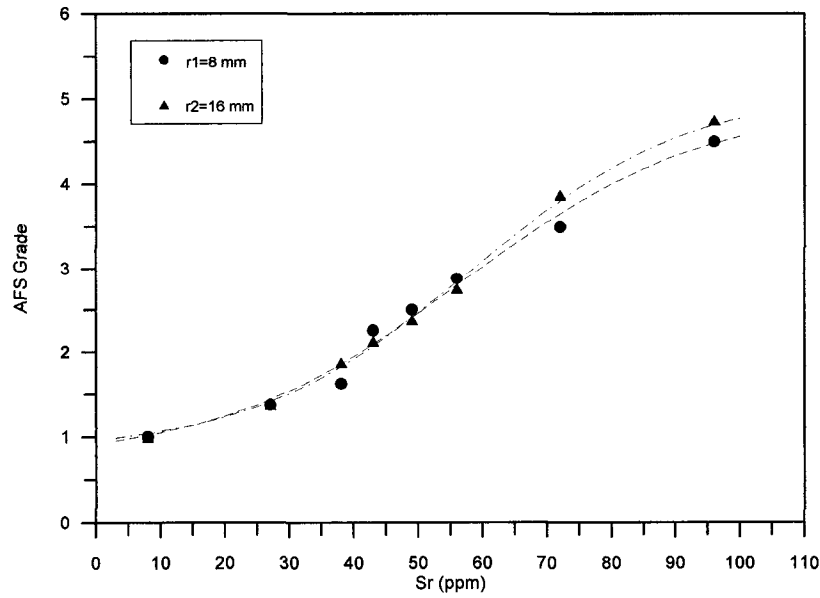


Figure 5.5 – Comparison of AFS Grade value vs. Sr addition for the wall and centre location [19].

Figure 5.6 depicts the relationships between Sr level, ΔT and AFS Grade for the AITAS test samples.

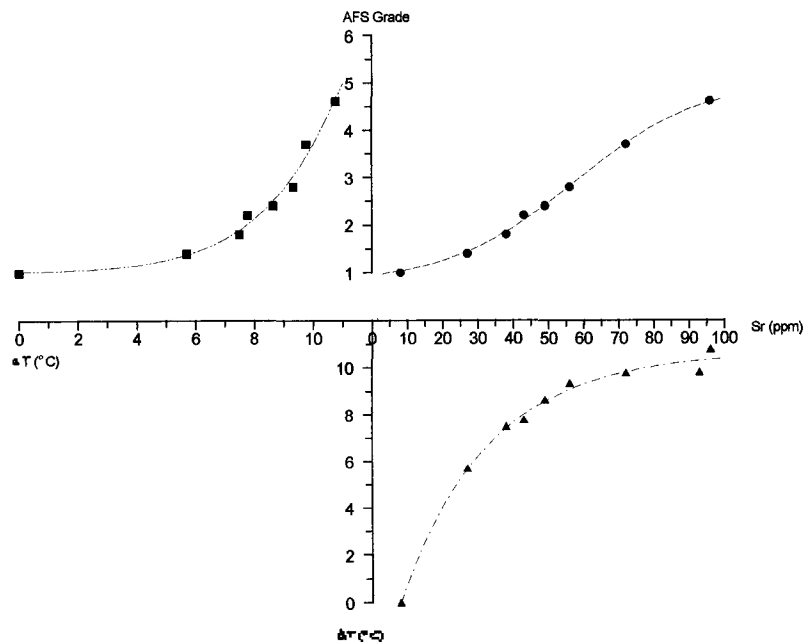


Figure 5.6. – Comparison of ΔT vs. Sr addition and AFS grade value [19].

5.3.4. Conclusions

1. The ALTAS accurately quantifies the degree of AlSi eutectic modification based on AFS specifications and can evaluate the degree of Sr fading over time.
2. There is a strong statistical correlation between the Sr level, ΔT and the AlSi eutectic modification level.

Chapter 6. The Effect of Strontium on the Formation of Al-Cu Phases

6.1. Literature Search

The melting temperature of AlCu rich phases determines the maximum temperature that 319 aluminum alloys can be exposed to during thermal sand removal (TSR) or solution treatment without incurring incipient melting. Up to three distinct AlCu phases can form during the process of 319 alloy solidification. These are a high Cu phase (approx. 40% wt%Cu), a medium Cu phase (up to 30 wt% Cu) and a low Cu phase (approx. 8wt% Cu). These phases can also contain other elements such as Mg (up to 4 wt%) and Si (up to 12 wt%). IRC research [12] and the existing literature [20-24] suggests that the Sr level has an influence on the formation of these phases. However, the precise effect that Sr has on the type of phase formed, its area fraction, solidification characteristics (e.g. nucleation and solidus temperature) and melting behaviour has yet to be determined.

The ALTAS system is capable of determining the general nucleation and solidus temperature for all of the Al-Cu rich phases present in the test sample structure based on cooling curve data (although it can not distinguish individual phases). However, to avoid the problem of incipient melting, it is important to know the melting temperature of the last phase to solidify. Previous IRC work has demonstrated that it is possible to measure this temperature using ALTAS data gathered during the heating cycle. This study showed that the incipient melting temperature was approximately 15 °C higher than the solidus temperature in low Sr level alloys due to the thermal hysteresis effect.

6.2. Experimental Work

Following is a portion of the work completed by the author in collaboration with Dr. M. Djurdjevic under the supervision of Dr. J. Sokolowski. This work looked at the effect of strontium on the copper eutectic as contained in the paper entitled “The Effect of Strontium on the Microstructure of the Aluminum-Silicon and Aluminum Copper Eutectics in the 319 Aluminum Alloy”. In addition, further work was done on the effect of copper content in Al-Si 3xx series of alloys in collaboration with Dr. C. Cacers and Dr. M. Djurdjevic.

6.2.1. Objective

1. To quantify the influence of the Sr level on the following characteristics of the AlCu rich phases: type and area fraction, nucleation and solidus temperature.

6.2.2. Experimental Procedure

WAP 319 aluminum alloy ingots produced by Alchem were used in this experiment. The ingots were melted in an electric resistance furnace and kept at a temperature of 730 +/- 5 °C. The melt was degassed for 15 minutes using an argon lance, however, no protective atmosphere was utilized during melt holding. It was then modified through the addition of 10% Sr master alloy. An incubation time of 15 minutes was allowed prior to

collecting the first sample. These samples were then taken by submerging a cylindrical graphite cup (40mm in diameter, 50mm deep) into the melt.

Light optical microscopy specimens were cut from the test samples close to the tips of the thermocouples.

6.2.3. Results

SEM/EDS analysis revealed the presence of three different AlCu rich phases: high, medium and low Cu phases as represented in Figure 6.1a,b. These phases contain some additional elements.

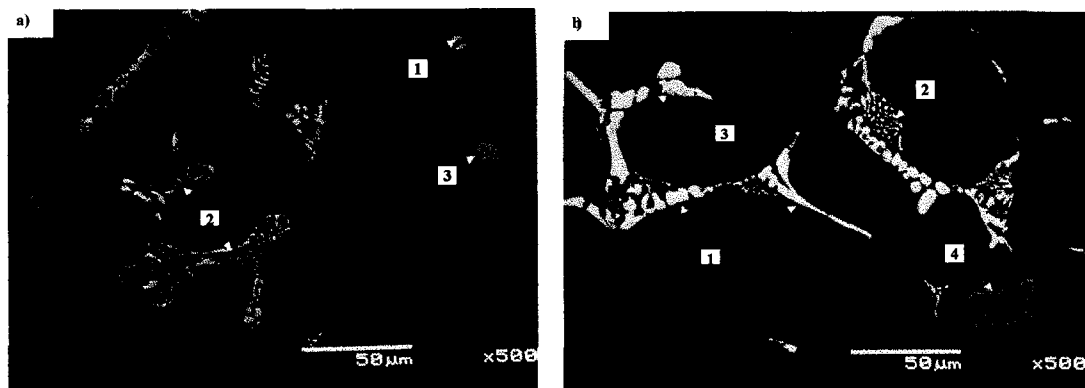


Figure 6.1 – SEM micrographs (BSE mode) samples with a) 8ppm and b) 96 ppm Sr, respectively. 1 - blocky Al₂Cu eutectic, 2 – eutectic Al-Al₂Cu, 3 – fine Al₅Mg₈Cu₂Si₆ eutectic types of copper phases, and 4 – iron phase [12].

Figure 6.2 shows that the addition of Sr decreases the area fraction of the medium Cu phase from 1.3 to 0.14% while increasing the high and low Cu phases from 0.44 up to 1.9%.

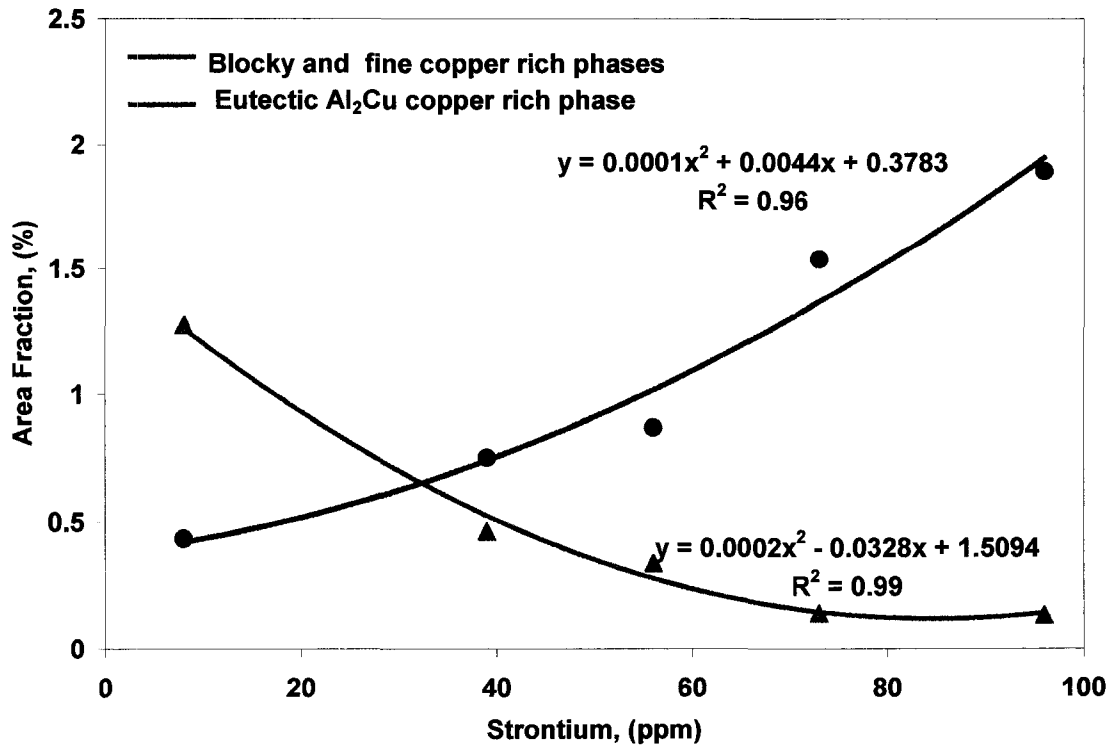


Figure 6.2 – Area fraction of Cu phases as a function of Sr content [12].

The Al-Cu eutectic nucleation temperature increased from approximately 504°C to 512°C when the Sr level was increased from 8 to 96 ppm. See Figure 6.3. This addition of Sr also increases the solidus temperature from approximately 486°C to 496°C. It is interesting to note that the solidus temperature rises approximately 30 ppm Sr and then becomes essentially stable.

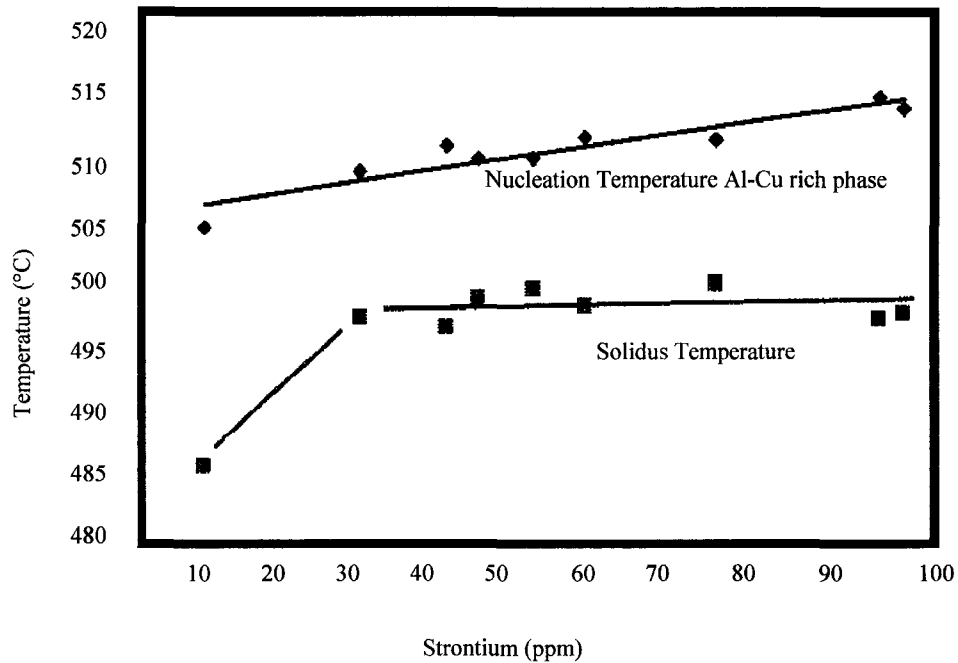


Figure 6.3 – Nucleation temperature of Al-Cu rich phases and solidus temperature compared to Sr content [12].

6.2.4. Conclusions

1. Increasing the Sr level increases the area fraction of the high Cu phase and the low Cu phase while decreasing the area fraction of the medium Cu phase.
2. The peaks on the first derivative of the cooling curve pertaining to the individual Al-Cu rich phases are convoluted. Consequently, the ALTAS system is unable to distinguish them. At present, only a general nucleation and solidification temperature of all the AlCu rich phases is reported.

Chapter 7 Modeling of Fraction Solid

7.1. Literature Search

Fraction solid is defined as the percentage of solid phase(s) that precipitates between the liquidus and solidus temperature in a solidifying melt. In order to make reliable predictions on casting structure and feedability, accurate information is required on the fraction solid.

Several methods of determining the fraction solid of a solidifying melt are presented in literature [25-35]. The most common technique employs quantitative metallography in which melt specimens are quenched between the liquidus and solidus temperatures. The volume fraction of phases present prior to quenching are measured and related to the solid fraction at the time of quenching. Thermal analysis has also been used to calculate the fraction solid. Using this method, the amount of heat evolved during the solidification of the test sample is related to the fraction solid. Differential thermal analysis and differential scanning calorimetry have also been used to determine the fraction solid. However, these methods require complicated and expensive instrumentation. Models available from the literature which calculate the fraction solid based on parameters derived from the fundamental analysis of the solidification process are displayed in Table 7.1.

Table 7.1 - Review of models for calculation of fraction solid [36].

No	TYPE OF MODELS	COMMENTS
1.	<p>LINEAR[1]</p> $f_S = \frac{T_{LIQ} - T}{T_{LIQ} - T_{SOL}}$ <p>T_{LIQ}- Liquidus temperature, °C T_{SOL}- Solidus temperature, °C T - Instantaneous temperature, °C</p>	<p>Latent heat is assumed to vary linearly between liquidus and solidus temperatures. This model has no theoretical basis, but is frequently used due to its simplicity.</p>
2.	<p>LEVER RULE [1]</p> $f_S = \frac{1}{1-k} \cdot \frac{T_{LIQ} - T}{T_m - T}$ $k = \frac{T_m - T_{LIQ}}{T_m - T_{SOL}}$ <p>k-Distribution coefficient of binary alloys T_m-Melting temperature of pure aluminum</p>	<p>Solidification in this model is assumed to progress very slowly and the solid and liquid phases coexist in equilibrium in the mushy zone.</p>
3.	<p>SCHEIL'S [1]</p> $T^{AlSi}_{E,G} < T < T_{LIQ}: \quad f_S = 1 - \left(\frac{T_m - T}{T_m - T_{LIQ}} \right)^{\frac{1}{k-1}}$ $T = T^{AlSi}_{E,G}: \quad f_S = 1$	<p>In this model it is assumed that no solute diffusion occurs in the solid phase and also that the liquid is perfectly homogeneous.</p>
4.	<p>GRAIN NUCLEATION [3,8]</p> $f_S = 1 - \exp\left(-\frac{4}{3} \cdot \pi \cdot R^3 \cdot N\right)$ <p>R-Average grain radius, m N-Average grain density, m⁻³</p>	<p>The calculation of fraction solid is based on the grain nucleation law and on the assumption that the shape of the grains is spherical.</p>
5.	<p>HEAT BALANCE [6,9,11]</p> $f_S = \frac{\int_0^t \left[\left(\frac{dT}{dt} \right)_{cc} - \left(\frac{dT}{dt} \right)_{zc} \right] dt}{\int_0^{ts} \left[\left(\frac{dT}{dt} \right)_{cc} - \left(\frac{dT}{dt} \right)_{zc} \right] dt} =$ $= \frac{C_p}{L} \cdot \int_0^t \left[\left(\frac{dT}{dt} \right)_{cc} - \left(\frac{dT}{dt} \right)_{zc} \right] dt$ <p>C_p-Specific heat of an alloy L-Latent heat of solidification dT/dt-Cooling rate</p>	<p>Fraction solid can be calculated by determining the cumulative area between the first derivative of the cooling curve (cc), and the "zero" cooling curve (hypothetical cooling curve without phase transformations) (zc).</p>

7.2 Experimental Work

Following is a portion of the work completed by the author in collaboration with Dr. M. Djurdjevic, Dr. W. Kierkus, G. Byczynski under the supervision of Dr. J. Sokolowski. This work proposed a new model for predicting the fraction solid based on key metallurgical reaction temperatures for the 319 aluminum alloy. This work has been published in a paper entitled “Modeling of Fraction Solid for the 319 Aluminum Alloy”.

7.2.1. Objective

1. To develop a model for the prediction of fraction solid based on key metallurgical reaction temperatures for the 319 aluminum alloy.

7.2.2. Experimental Procedure

319 aluminum alloy ingots obtained from WAP were melted under a protective nitrogen atmosphere using a heat resistance furnace. A graphite cup (40mm diameter, 50mm eight) was submerged into the melt to collect the sample. No further melt treatment was performed. A total of twelve samples were collected to assure reproducibility and repeatability of the results. The average chemical composition of the samples is summarized in Table 7.2. The melt temperature was held at 730 °C ($\pm 5^\circ\text{C}$). The thermal analysis was performed using the Fluke Netdaq data acquisition system with N-type thermocouples.

Table 7.2 – Average chemical composition of 319 aluminum alloy [36].

Element	Si	Cu	Mg	Mn	Zn	Ti	Fe	Sr
Wt. %	7.35	3.21	0.29	0.23	0.15	0.12	0.40	0.0025

7.2.3. Results

Experimentally obtained values for the distribution of fraction solid with respect to temperature will be used in the this work for developing a new model for calculation of fraction solid. However, before the numerical method for calculation of fraction solid is described it is necessary for the cooling curve to be analyzed.

According to Figure 7.1 the temperature range between liquidus and solidus can be separated into three distinct segments. Each segment is related to distinct metallurgical reactions that occur during solidification of the 319 alloy. Table 7.3 gives the temperature boundaries for characteristic metallurgical reactions pertinent to each segment.

Table 7.3 – Segmentation of cooling curve [36].

Segment of the cooling curve	Boundary conditions	Metallurgical reactions
I	$T_{LIQ} \geq T > T_{E,G}^{AlSi}$	Nucleation and growth of α - aluminum dendrite network, dendrite thickening.
II	$T_{E,G}^{AlSi} > T > T_{E,G}^{AlCu}$	Nucleation and growth of Aluminum-silicon eutectic.
III	$T_{E,G}^{AlCu} > T > T_{SOL}$	Nucleation and completion of aluminum copper-reaction and solidification process.

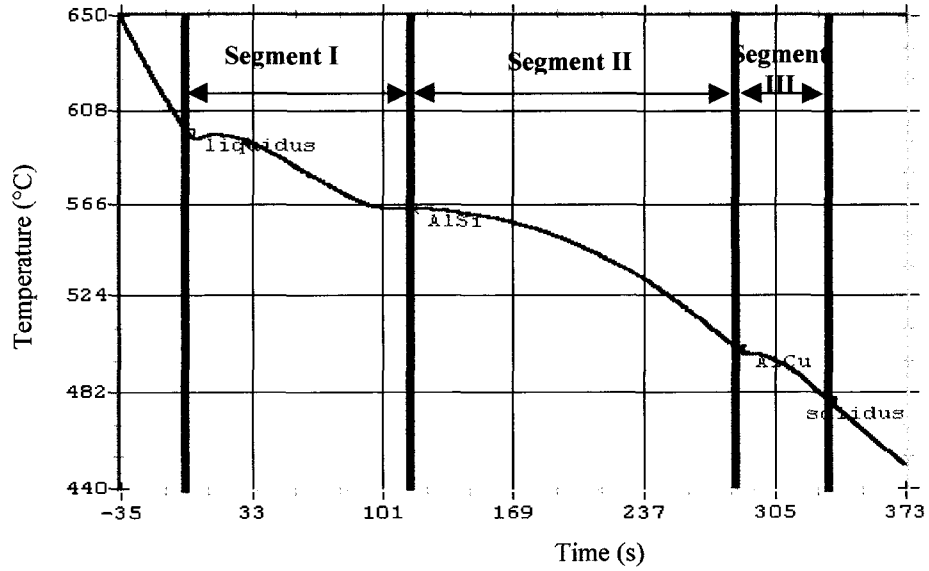


Figure 7.1 – Cooling curve of 319 aluminum alloy [36].

During the first segment of solidification process, fraction solid versus temperature can be expressed by equation 7.1.

$$f_s^I = (T_{LIQ} - T) / (T_{LIQ} - T_{E,G}^{AlSi})^{n1} f_s^{AlSi} \quad (7.1)$$

Where: f_s^I – fraction solid, varying between 0 and f_s^{AlSi} ;

f_s^{AlSi} – fraction solid at the aluminum-silicon eutectic growth temperature;

T_{LIQ} - liquidus temperature (nucleation of α - aluminum dendrites);

T – running temperature between T_{LIQ} and $T_{E,G}^{AlSi}$;

$T_{E,G}^{AlSi}$ – aluminum-silicon eutectic growth temperature;

$n1$ – nonlinear factor.

The relationship between fraction solid and temperature in the second segment of the cooling curve may be described by equation (7.2):

$$f_s^{II} = f_s^{AlSi} + (T^{AlSi}_{E,G} - T)/(T^{AlSi}_{E,G} - T^{AlCu}_{E,G})^{n2} (f_s^{AlCu} - f_s^{AlSi}) \quad (7.2)$$

Where: f_s^{II} – fraction solid, varying between f_s^{AlSi} and f_s^{AlCu} ;

f_s^{AlCu} – fraction solid at the aluminum-copper eutectic growth temperature;

$T^{AlCu}_{E,G}$ – aluminum copper eutectic growth temperature;

T – running temperature between $T^{AlSi}_{E,G}$ and $T^{AlCu}_{E,G}$;

$n2$ – nonlinear factor.

Equation (7.3) describes the relationship between fraction solid and temperature in the third segment of the cooling curve:

$$f_s^{III} = f_s^{AlCu} + (T^{AlCu}_{E,G} - T)/(T^{AlCu}_{E,G} - T_{SOL})^{n3} (100 - f_s^{AlCu}) \quad (7.3)$$

Where: f_s^{III} – fraction solid, varying between f_s^{AlCu} and 100%;

T_{SOL} – solidus temperature;

$n3$ – nonlinear factor.

The procedure for calculating fraction solid used in this work is based on a concept presented by K. G. Upadhyya et al. [32], and H. Huang et al. [30]. In their research on 356 alloy, T_{LIQ} and T_{SOL} temperatures were taken from graphs depicting fraction solid as

a function of temperature, while the aluminum-silicon eutectic growth temperature was taken from Baekkerud's work [24].

In order to calculate the fraction solid, two coefficients from equations 3 to 5, f_s^{AlSi} and f_s^{AlCu} , were derived from the experimental data using the heat balance equation. The non-linear factors (n1, n2 and n3) were not known and thus were matched to the experimental data using least squares regression analysis. For the 319 alloy the numerical values of these coefficients and factors are listed in Table 7.4.

Table 7.4 - Numerical values for f_s^{AlSi} and f_s^{AlCu} and nonlinear factors (n1, n2 and n3), for the 319 alloy [36].

Factors	f_s^{AlSi} , (%)	f_s^{AlCu} , (%)	n1	n2	n3
	46.60	92.54	0.80	0.20	0.30

Figure 7.2 compares the fraction solid – temperature relation described by the different models presented in the literature with the model presented in this work. Table 7.5 compares the fraction solid calculated according to the author's model with Backerud's results [24].

Table 7.5 - A comparison of fraction solid calculated according to the present model with that of Backerud [36].

University of Windsor Model		Backerud's experimental data [24]	
Temperature, (°C)	Fraction solid, (%)	Temperature, (°C)	Fraction solid, (%)
604.6	0	604.0	0
600.0	7.8	600.0	12.0
579.0	31.0	579.0	35.0
561.0	67.6	561.0	51.0
507.0	95.2	507.0	94.0
495.0	98.6	495.0	100.0

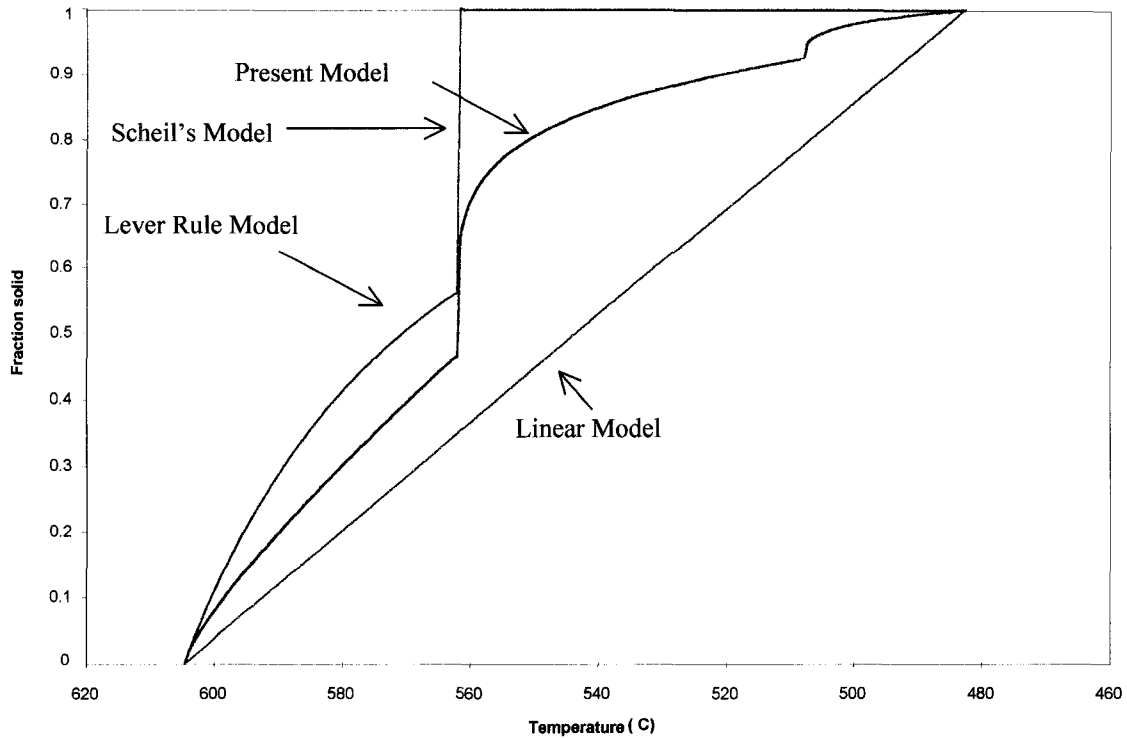


Figure 7.2 - Fraction solid as a function of temperature for the various models [36]

The different fraction solid estimates calculated according to Backerud's model and the present model can be attributed to differences in the chemical compositions of the 319 alloy used in the two studies (compare Table 7.2 with Table 7.6).

Table 7.6 - Chemical composition of the 319 aluminum alloy used in Backerud's study [36].

Element	Si	Cu	Mg	Mn	Zn	Ti	Fe	Sr
Wt. %	6.08	3.27	0.05	0.33	0.66	0.14	0.64	NA

7.2.4. Conclusions

1. A model for calculating fraction solid versus temperature, based on the thermal analysis technique, was developed in this work.
2. The original cooling curve showed that the temperature range between the liquidus and solidus temperature could be separated into three distinct segments. For each segment, a model for calculating the fraction solid was developed as a function of temperature.

Chapter 8. Conclusions and Recommendations

Thermal analysis is an excellent tool for the quantification of the 319 aluminum alloy microstructure.

Improved filtering techniques have improved the use of higher order derivative curves. This allows for more precise automatic determination of characteristic temperatures during solidification, which reduces the required interaction between the user and the software.

The investigation of increasing strontium in 319 aluminum alloy showed that AITAS is capable of determining the degree of silicon modification. However, more experimental work is needed to understand what influences other alloying elements such as antimony, bismuth etc. have on the effectiveness of strontium as a modifier.

Investigating the effect of strontium on the morphology of the Al-Cu phases demonstrated that AITAS has the ability to determine which Al-Cu phases are present including the area fraction. Further work is required to determine the nucleation temperatures of the individual Al-Cu phases by the deconvolution of the Copper peaks found on the cooling curve.

REFERENCES:

- [1] Aluminum Casting Technology (1993) *AFS Publications*
- [2] ASM Handbook (1992) *ASM International*
- [3] Murray, J. and McAlister, A.J. (1984) The Al-Si System, *Bulletin of Alloy Phase Diagrams*, vol.5
- [4] Mackay, R.I. (1998) Personal Communication, McGill University
- [5] Savitzky, A. and Golay, M. J. E. (1964) Smoothing and Differentiation of Data by Simplified Least Squares Procedures, *Analytical Chemistry*, vol. 36
- [6] Mondolfo, L.F. (1983) *Grain Refinement in Castings and Welds*, Butterworths, London, p.3
- [7] McCartney *International Metallurgy*, vol.89, p.247-260
- [8] Sigworth, G.K. (1984) *Metallurgical Transactions*, vol. 15A, p. 223-234
- [9] Chai, G. (1994) *Dendrite Coherency During Equiaxed Solidification in Aluminum Alloys*, Ph.D. Thesis, Stockholm University
- [10] Gruzleski J.E. and Ananthanarayanan, L. (1984) *AFS Transactions*, vol. 92, p. 383-391
- [11] A Pacz-Patent USA (1920) no. 1.387.900
- [12] Djurdjevic, M., Stockwell, T., and Sokolowski, J. The Effect of Sr on the Microstructure of the Al-Si and Al-Cu Eutectics in the 319 Aluminum Alloy, *International Journal of Cast Metals Research*, In Press
- [13] Zindel, J. and Boileau, J. (1996) Ford Research Laboratory, *TMS Fall Meeting*, p.20.
- [14] Crossley, P.B. and Modnolfo, L.F. (1966) *Modern Casting*, vol. 49, p.63
- [15] Apelian, D., Sigworth, G., and Whaler, K. (1984) *AFS Transactions*, vol. 92, p.297
- [16] Argyropoulos, Closset, B., Gruzleski, J.E., and Oger, H. (1983) *AFS Transactions*, Vol.91, p.351

- [17] Closset, B., Pirie, K., and Gruzleski, J.E. (1984) Comparison of Thermal Analysis and Electrical Resistivity in Microstructure Evaluation of Al-Si Foundry Alloys, *AFS Transactions*, vol.92, p. 122-133
- [18] Honer, K.E. (1982) *Foundry Management & Technology*, vol. 10, p.50-53
- [19] Apielian, D. and Cheng, J.A. (1986) Al-Si Processing Variables: Effect of Grain Refinement and Eutectic Modification, *AFS Transactions*, vol. 94, p.797-808
- [20] Doty, H.W., Samuel, A.M., and Samuel, F.H. (1996) Factors Controlling the Type and Morphology of Copper-Containing Phases in the 319 Aluminum Alloy, *100th AFS Casting Congress*, Philadelphia, Pennsylvania, USA
- [21] Samuel, A.M. and Samuel, F.H. (1995) A Metallographic Study of Porosity and Fracture Behavior in Relation to the Tensile Properties in the 319.2 Chill Casting, *Metallurgical Transactions*, vol. 26A, p. 2359-2372
- [22] Mulazimoglu, M., Tenekedjev, N., Glosset, B., and Gruzleski, J. (1995) *Microstructures and Thermal Analysis of Strontium Treated Al-Si Alloys*, American Foundrymen's Society Inc., Des Plaines, USA, p.23-40
- [23] Gathier, J., Louchez, P., and Samuel, F. (1995) Heat Treatment of 319.2 Aluminum Automotive Alloy, *Cast Metals*, vol. 8, p. 91-114
- [24] Bäckerud, L., Chai, G., and Tamminen, J. (1986) *Solidification Characteristics of Aluminum Alloys*, American Foundrymen's Society Inc., Des Plaines, USA, p. 95-105
- [25] Flemings, M.C. (1972) *Solidification Processing*, McGraw-Hill Inc., p.60-166
- [26] Ohta, S. and Asai, K. (1993) The Behaviour of Temperature Decreasing and Fraction Solid Increasing in Solid-Liquid Coexisting Zone in Solidification Process of Aluminum Alloy Weld Metal, *Transactions of the Japan Welding Society*, vol. 24, p. 131-139
- [27] Saunders, N. (1996) Phase Diagram Calculations for Commercial Al-Alloys, SF2M and INPG, *Material Science Forum*, vol. 222, p. 667-672
- [28] Chen, J.H. and Tsai, H.L. (1990) Comparison of Different Models of Latent Heat Release for Modelling Casting Solidification, *AFS Transactions*, vol. 98, p.539-546
- [29] Kantekar, C.S. and Stefanescu, D.M. (1988) Macro-Micro Modelling of Solidification of Hypoeutectic and Eutectic Al-Si Alloys, *AFS Transactions*, vol. 60, p.591-598

- [30] Huang, H., Suri, V.K., Hill, J.L., and Berry, J.T. (1991) Heat Source/Sink Algorithm for Modeling Phase Changes During Solidification in Castings and Water Evaporation in Green Sand Molds, *AFS Transactions*, vol. 54, p. 685-689
- [31] Rapaz, M. (1989) Modeling of Microstructure Formation in Solidification Processes, *International Materials Reviews*, vol. 34, p.93-123
- [32] Upadhy, K.G., Stefanescu, D.M., Lieu, K., and Yeager, D.P. (1989) Computer-Aided Cooling Curve Analysis: Principles and Applications in Metal Casting, *AFS Transactions*, vol. 47, p. 61-66
- [33] Stefanescu, D.M., Upadhy, G., and Bandyopaadhyay, D. (1990) Heat Transfer-Solidification Kinetics Modeling of Solidification of Castings, *Metallurgical Transactions*, vol. 21A, p. 997-1005
- [34] Kurz, W. and Fisher, D.J. (1986) *Fundamentals of Solidification*, Trans Tech Publications, U.K.-USA, p.149-152
- [35] Jeng, S. and Chai, S. (1996) Determination of the Solidification Characteristics of the A356.2 Aluminum Alloy, *Material Science Forum*, vol. 217, p. 283-288
- [36] Djurdjevic, M., Kierkus, W., Byczynski, G., Stockwell, T., and Sokolowski, J. Modelling of Fraction Solid for the 319 Aluminum Alloy, *AFS Transactions*, In Press
- [37] Mondolfo, L.F. (1979) *Aluminum Alloys, Structure and Properties*, Butterworths, London, p. 213-614
- [38] Reed-Hill, R.E., Abbaschian, R. (1994) *Physical Metallurgy Principals*, PWS Publishing

Appendix A
AITAS Training Manual

Aluminum Thermal Analysis System (ALTAS)

System Training

Author: T. Stockwell

Overall Objectives

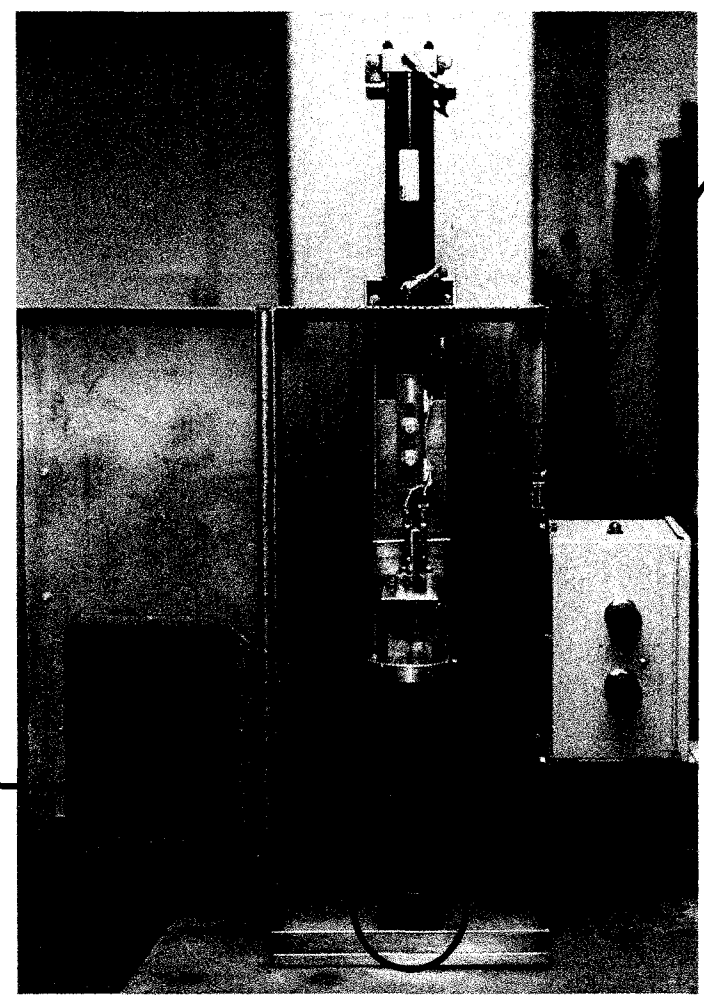
- *Identify and control the modification level of the Aluminium Silicon Eutectic phase.*
- *Establish a relationship between the test sample solidification characteristics and relate these relationships to actual castings properties.*

ALTAS Hardware

The Ford WAP Stand

Top of
stand.
Amber
Warning
light

Self alignment
ceramic cup
holder



K-type
Thermocouple
Assembly

Control Panel

ALTAS Hardware

The Stand

- 1 *Contains the location of the raw data file and calibration files used.*
- 2 *Contains information on the operator and time and date of the test.*
- 3 *Displays the specifications regarding the maximum and minimum temperatures recorded and the sampling frequency.*
- 4 *Displays all the characteristic temperatures ($^{\circ}\text{C}$), time (s), fraction solid (%) and cooling rate ($^{\circ}\text{C}/\text{s}$).*
- Δ *Displays the AlSi eutectic temperature depression ($\Delta T^{\text{Al-Si}}_{\text{E,G}}$). This number is used as an indicator of the level of modification.*
- 6 *Displays the AFS number that characterises the level of silicon modification.*

ALTAS Hardware

The Consumables

- *Graphite cup*
 - *replacement required every 30 trials or upon damage*
- *Stainless steel sheaths*
 - *must be replaced every trial*
- *Calibrated K - type thermocouple probes*
 - *replacement required once a month*

Sampling Procedure

In order to ensure an unbiased test sample structure, the following procedure is recommended:

- *Follow all safety measures, which include wearing all safety equipment and observing all safety rules associated with the handling of molten aluminum.*
- *Place the AITAS stand as close as possible to the sampling point in a location that is free from vibration.*
- *Verify the installation of thermocouple stainless steel sheaths.*
- *Pre-heat the thermal analysis graphite cup by placing it near the molten metal so that it will be free of moisture during sampling in order to prevent a rapid temperature change of the test sample.*
- *Just before sampling, skim off the surface of the liquid metal well.*
- *Immerse the thermal analysis cup into the metal at an angle of approximately 45° in order to avoid incorporating oxides into the sample.*
- *Hold the thermal analysis cup 4 to 6 inches under the surface of molten aluminum for 15 seconds in order to equalise the temperature of the graphite cup.*
- *Withdraw the thermal analysis cup to collect the test sample.*

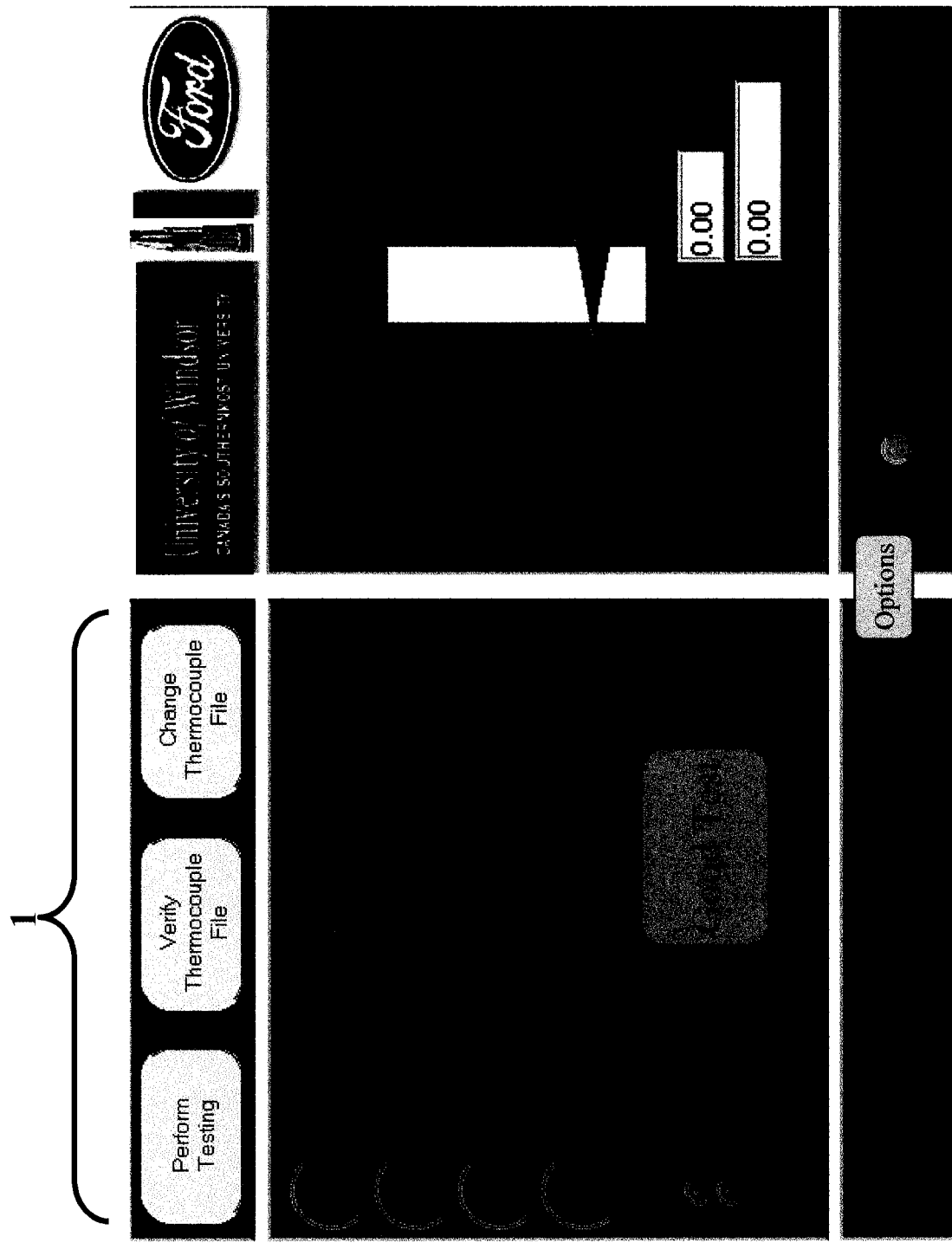
Sampling Procedure Continued

- *Place the thermal analysis cup on the ceramic holder within the AITAS stand. MAKE SURE THE CUP IS LOCATED PROPERLY in the self alignment hole.*
- *Close the AITAS cabinet door and lower the thermocouple assembly by pressing the green “Start Button” (must hold until in the down position).*

To Remove a Sample:

- *Upon completion of a test, press the red “Stop Button”, which will raise the thermocouple assembly. The test sample and cup will remain attached to the assembly.*
- *Remove the graphite cup using the appropriate tongs. CAUTION: THE CUP WILL REMAIN HOT (~400°C).*
- *After the removal of the cup, grasp the sample with the tongs and pull straight down. This is important in order to avoid bending the thermocouples.*
- *Replace stainless steel thermocouple sheaths.*

ALIAS Software Main Screen



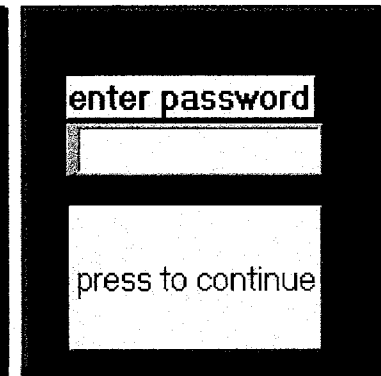
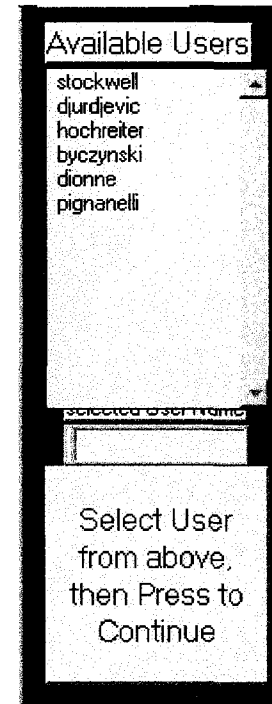
ALTAS Software

Main Screen

1. *Main control module*
 - *allows the user to either perform a test or verify/change the thermocouple calibration information.*
2. *Status module*
 - *displays the current status of the ALTAS software*
3. *Analysis module*
 - *displays the AISi Eutectic temperature, depression of the AISi eutectic temperature compared to an unmodified 319 and the level of modification (AFS number).*
4. *Thermocouple error indicator*
 - *notifies the user of a disconnected thermocouple*
5. *Successful Test Indicator*
 - *Informs the user on whether the test was performed successfully.*
6. *Advanced Options Button*
 - *access to advanced cooling curve manipulation and administrator tasks*

AITAS Software Program - Logging In

- *Upon pressing the “Perform Testing” button the user will be prompted to enter a user name followed by a password. The user name can be selected out of a available user list by pressing the left mouse button over the desired name.*
- *If an improper user name or password is entered, the system will prompt the user to re-enter the information up to 3 times where by it resets.*
- *Upon completion of the logging in procedure, the system will prompt the user to insure that the protective thermocouple sheaths are in place. After selecting “Continue”, the system is ready to start collecting data. This is demonstrated by a flashing light on the top of the AITAS control box.*



ALIAS Software

Verification of Thermocouples

The screenshot displays the ATIAS software interface for thermocouple verification. At the top, there are three buttons: "Perform Testing", "Verify Thermocouple File", and "Change Thermocouple File". Below these buttons are two input fields for calibration file names:

- Tc Cal. Filename: %c:\netdaq\calibrate\tc971204cl.cal
- Tw Cal. Filename: %c:\netdaq\calibrate\tc971204wl.cal

At the bottom of the interface, there are two numerical input fields, both containing the value "0.00". A "Press to Continue" button is located below the input fields. In the top right corner, there is an "Options" button. The background of the interface features the University of Windsor logo and the Ford logo.

AITAS Software

Verification of Thermocouples

Procedure for handling thermocouple calibration information:


- *Upon receiving calibrated thermocouples, the identification number and calibration information will be entered using the AITAS "Calibration Information" program. These files will then be saved on the AITAS computer in the file folder named "Calibration".*
- *When a replacement thermocouple is needed, it is retrieved from the crib and inserted into the AITAS stand. Next the thermocouple change is recorded in the AITAS software using the "Change Thermocouple" button located on the main screen (for detailed instructions please see changing thermocouple, page --).*

"Verify Thermocouple File" button:

- *Upon pressing the "Verify Thermocouple File" button, a window will appear which gives the location and identification of the current thermocouples files loaded in the AITAS software.*
- *If there is and discrepancy between the thermocouple identification information loaded in the AITAS system and the thermocouples installed in the AITAS stand, corrections should be made immediately. This is done by selecting the continue menu and selecting the "Change Thermocouple" button on the main screen.*

ALTAS Software

Changing Calibration File

Perform Testing	Verify Thermocouple File	Change Thermocouple File	University of Windsor CANADA'S SOUTHERNMOST UNIVERSITY	
-----------------	--------------------------	--------------------------	---	---

Tc Filename	<input type="text" value="tc971204c1"/>
Tw Filename	<input type="text" value="tc971204w1"/>

Enter Calibration Filenames (NO extensions) Press Finished	<input type="text" value="0.00"/>	<input type="text" value="0.00"/>
--	-----------------------------------	-----------------------------------

Options

ALTAS Software

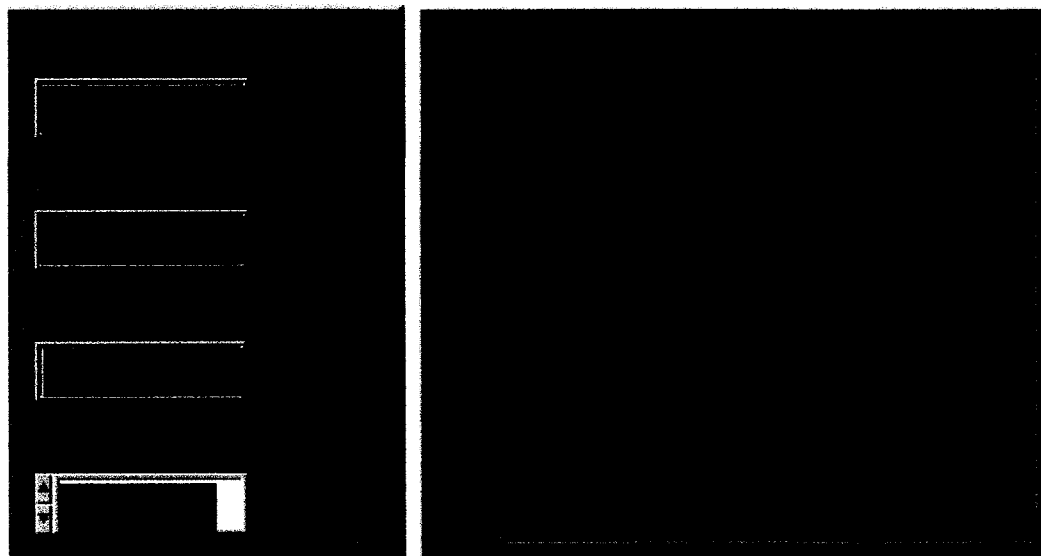
Changing Calibration File

“Change Thermocouple File” button:

- *Upon pressing the “Change Thermocouple File” button, a window will appear which gives the current identification loaded in the ALTAS software.*
- *If the information for either the centre or wall thermocouple is incorrect, replace the current information with the correct identification information.*
- *The thermocouple information is appended to the raw data file so it is important to ensure proper identification of the thermocouples in use.*

ALTAS Software

Collection of Data



- *As the system begins to record, a real time plot appears. This informs the user as to the current state of testing. In addition to the plot, the maximum temperature recorded is displayed. This temperature must be greater than 700°C in order to obtain reliable readings.*

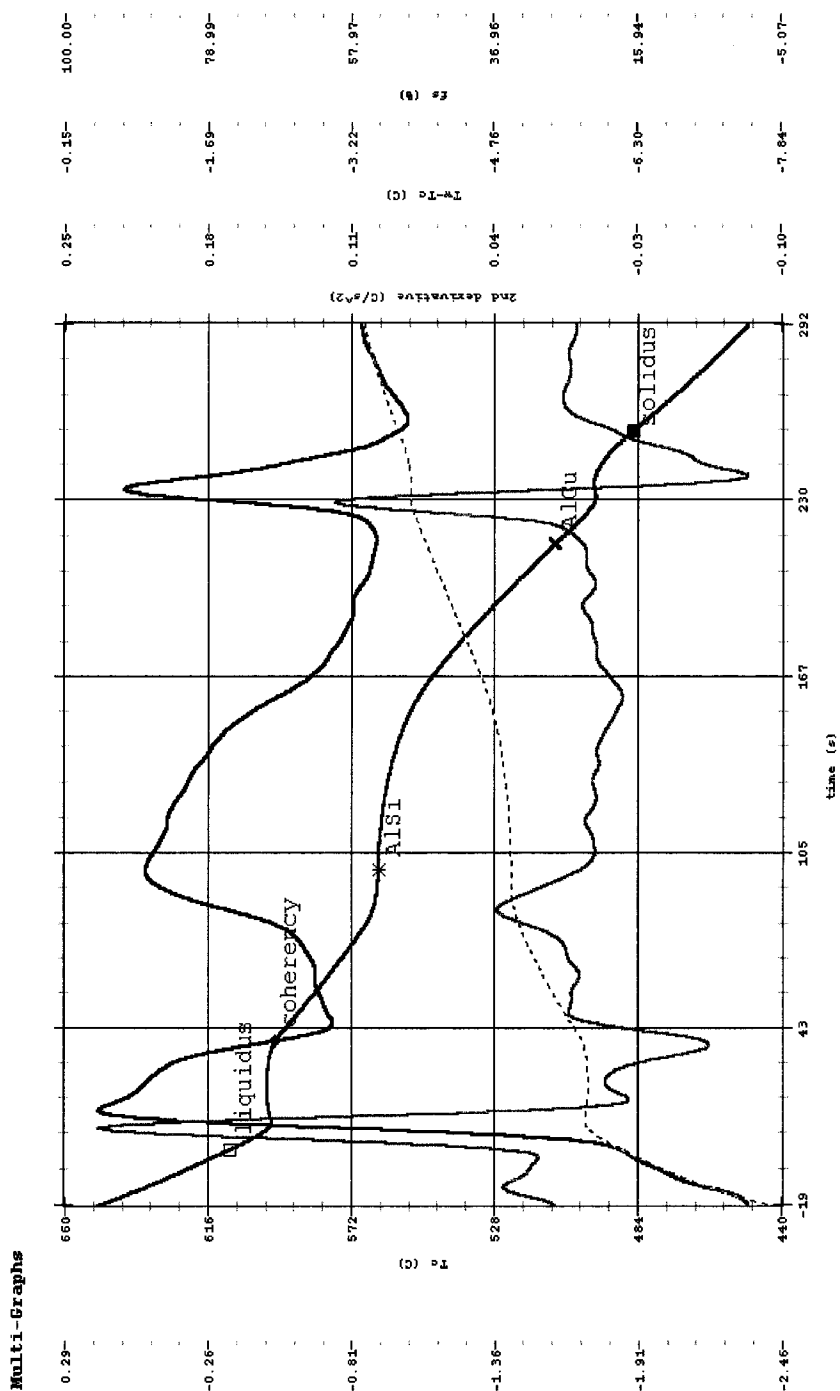
Analysis of Data

- *The determination of all the characteristic temperatures, dendrite arm spacing and grain size are all described in detail in the full report.*

Report Generation Data Portion

- 1 *Contains the location of the raw data file and calibration files used.*
- 2 *Contains information on the operator and time/date of the test.*
- 3 *Displays the specifications regarding the maximum and minimum temperatures recorded and the sampling frequency.*
- 4 *Displays all the characteristic temperatures ($^{\circ}\text{C}$), time (s), fraction solid (%) and cooling rate ($^{\circ}\text{C}/\text{s}$).*
- 5 *Displays the AlSi eutectic temperature depression, ($\Delta T^{\text{Al-Si}}_{\text{E,G}}$). This number is used as an indicator of the level of modification.*
- 6 *Displays the AFS number that characterises the level of silicon modification.*

Report Generation Graph Portion



Advanced ALTAS Capabilities

Options

The screenshot displays the ALTAS software interface with the following elements:

- Top Bar:** Ford logo, University of Windsor CANADA'S SOUTHERNMOST UNIVERSITY, and a New User button.
- Left Panel:** Three buttons: Perform Testing, Verify Thermocouple File, and Change Thermocouple File.
- Main Area:** A large dark area with a central white rectangular box and two smaller white boxes containing the value 0.00.
- Right Panel:** An Options button, a Run ALTAS WAP button, and several input fields with values: 2000, 680.00, 400.00, and 00:00:00.200.

Advanced ALTAS Capabilities

Options

- *By pressing the “Options” button, the user will be asked to enter a security password. After successfully entering the password, additional buttons and switches will become available. These include;*
 - 1 *The “Run previous files” button allows the user to re-analyse files in which they can zoom in on certain areas or view additional charts.*
 - 2 *The second group consists of sampling variables. These include the trigger temperatures. Trigger temperatures define when the data logger should start and stop recording data. In addition to the triggers, the user can also change the sampling frequency and maximum readings. For the current unit, the maximum data rate is 5 Hz per channel. Therefore 2000 scans or 4000 total readings is the default for the maximum number of readings.*

Advanced ALTAS Capabilities

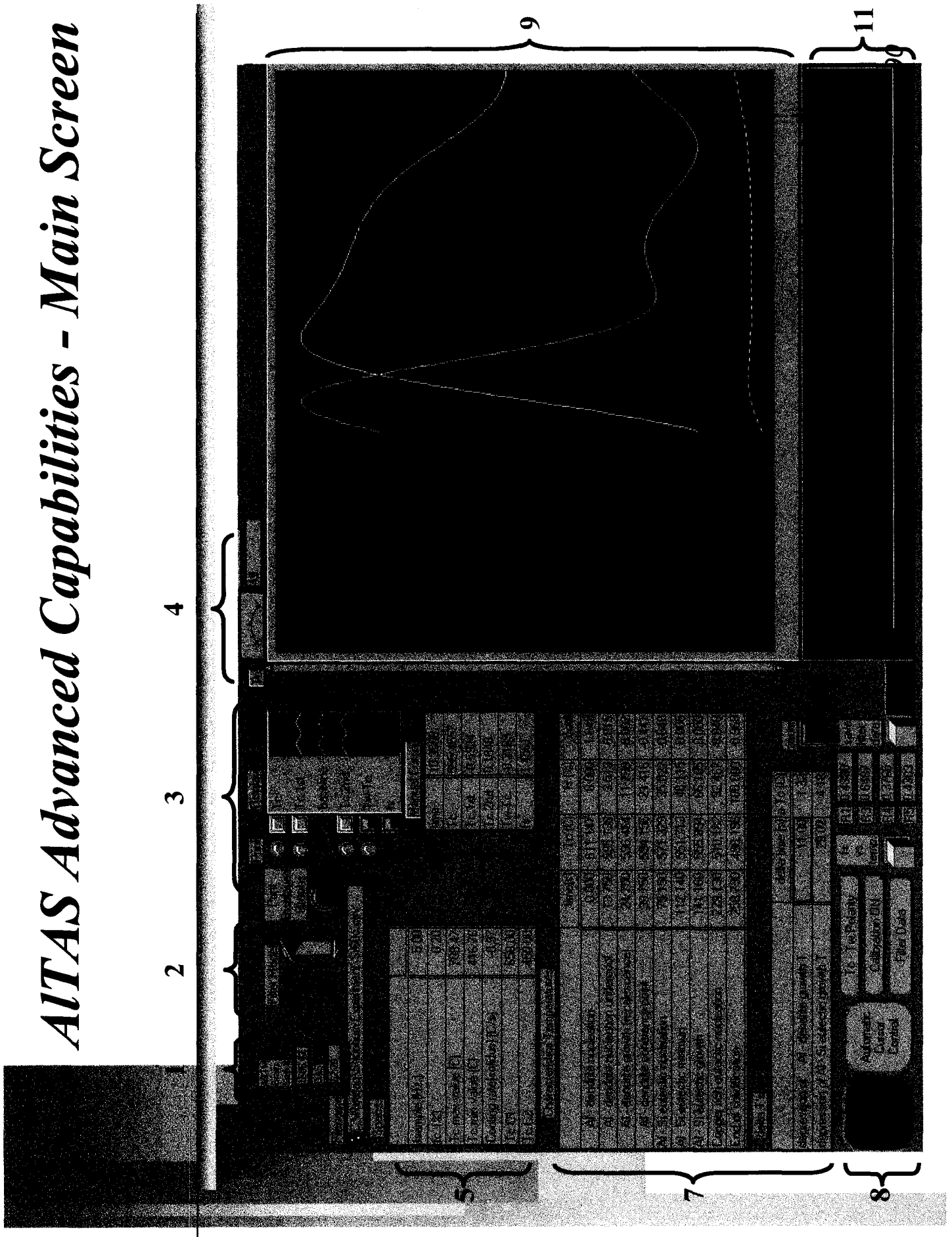
Options

- 3 *The “Run Continuous” switch must be in the “ON” position in order to allow the user to have manual control of the ALTAS software. This would be necessary if the user wanted to zoom in on a certain part of the curve or look at additional graphs. If the switch is in the “OFF” position, the user will simply re-evaluate the data and return to the initial main screen. This button should be in the “OFF” position during testing.*

- 4 *The “Print” switch in the “YES” position allows the user to automatically print the cooling curve and the 1st and 2nd derivative curves after each test or evaluation in the form of the general report. The “New User” button allows the user to add or remove user names and password information to the system.*

- 5 *The last module determines which filtering routine is used to reduce the noise in the original data. At the present time, the IRC suggests the Weighted Moving Average filter be used in order to eliminate the greatest amount of noise while still retaining the original shape of the curve.*

ALTAS Advanced Capabilities - Main Screen



AITAS Advanced Capabilities

Main Screen

- 1 *The first module reports the estimated ASTM grain size and dendrite arm spacing determined by the mathematical models presented in the detailed manual.*
- 2 *The second module again displays the filtering procedure used in reducing the noise. This must be set prior to running the program on the AITAS Main Screen.*
- 3 *Module 3 displays the legend for the accompanying graph as well as the print and display options. The large circular button under the heading “**Print Displayed Graphs**” will print the current curves shown on the graph (9) in the form of a general report. Next, smaller circular buttons under the heading “**Print**” will print only the corresponding curve in the form of a general report. Finally, square buttons control which curves are displayed on the graph (9).*
- 4 *Module 4 displays the number of iterations the program has performed. The AITAS software continues to iterate in order to allow the user to make changes to the display in a real time mode. It is recommended that eight iterations are performed before curve manipulation is performed.*

ALTAS Advanced Capabilities

Main Screen

- 5 *Module 5 displays the specifications obtained for the test. These include; the sampling frequency, maximum and minimum pour temperature (before filtering), the cooling rate and the maximum and minimum temperatures on the graph.*
- 6 *The manual cursor information is obtained in module 6. The manual cursor is located on the graph (9).*
- 7 *Module 7 list all the characteristic temperature information including time(s), temperature (°C), fraction solid (%) and cooling rate (°C/s).*
- 8 *When the system is in continuous running mode, the “**Press to Quit**” button must be used in order to return to the main ALTAS screen.*
- 9 *The main graph is used to display all the curves including the original cooling curve, 1st and 2nd derivative curves, ΔT curve ($T_c - T_w$), fraction solid and the baseline curve (the baseline curve is always displayed with the 1st derivative curve).*



ALTAS Advanced Capabilities

Zooming Capabilities

- *By pressing the “Zoom” button (10) an additional window appears with the entire cooling curve visible (11). Two boundary bars are present which determine which part of the cooling curve is shown on the main graph.*

Vita Auctoris

Todd J. Stockwell was born in 1973 in Windsor, Ontario, Canada. He attended the University of Windsor and obtained a Bachelor of Applied Science Degree in 1996. Todd has been an active member in many technical societies including the Society of Automotive Engineers, and the American Foundrymen where he currently holds the position of Vice Chairman of the Detroit Chapter. Todd has been an employee of the Ford Motor Company since joining the NSERC / Ford / University of Windsor Industrial Research Chair in Light Metals Casting in September of 1996.